Observations of ‘Classical’ dSph Galaxies: What’s in the Data

MG Walker & Jorge Peñarrubia (submitted to ApJ)

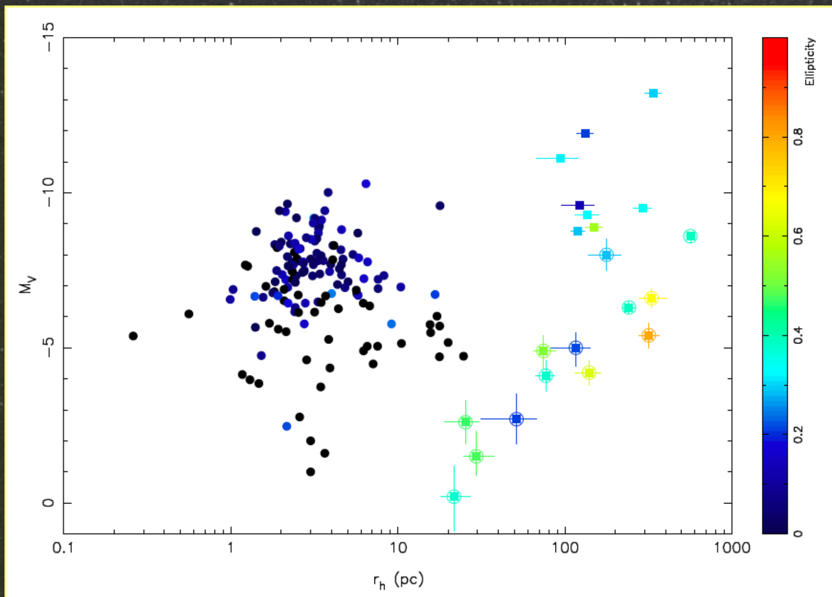

Belokurov et al. (2007), Gilmore et al. (2007), Martin et al. (2008)

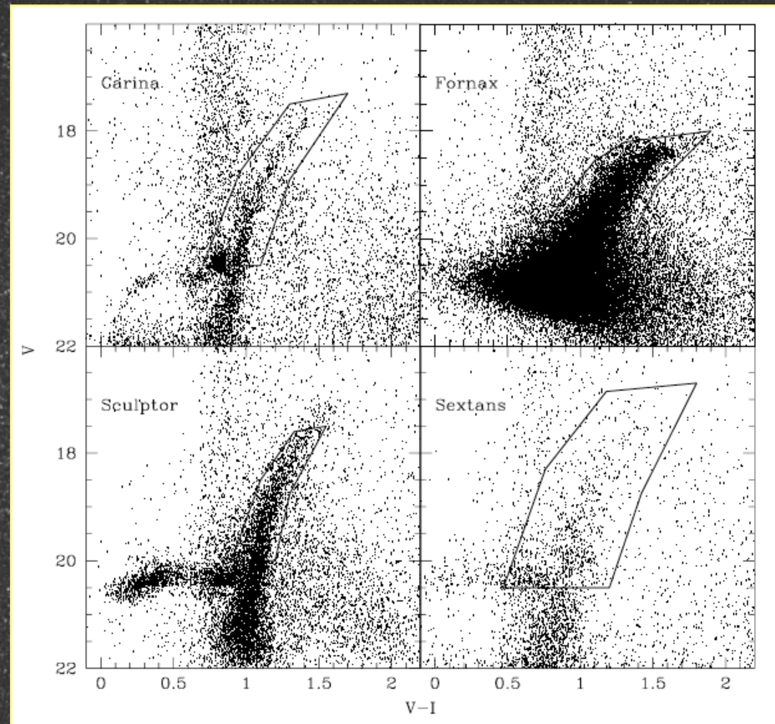

Dynamics of Low Mass Stellar Systems

ESO/Santiago, 5 April 2011

Spectroscopic Observations

w/ Mario Mateo & Ed Olszewski

(assist from Matt Coleman & Gary Da Costa)

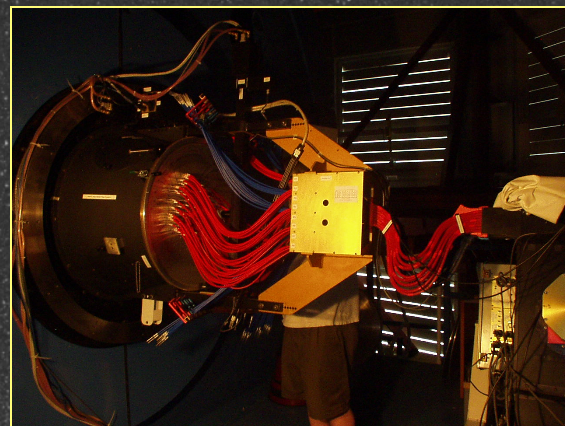

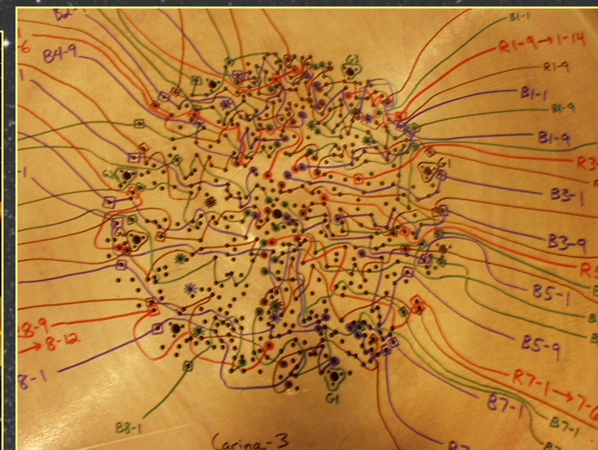

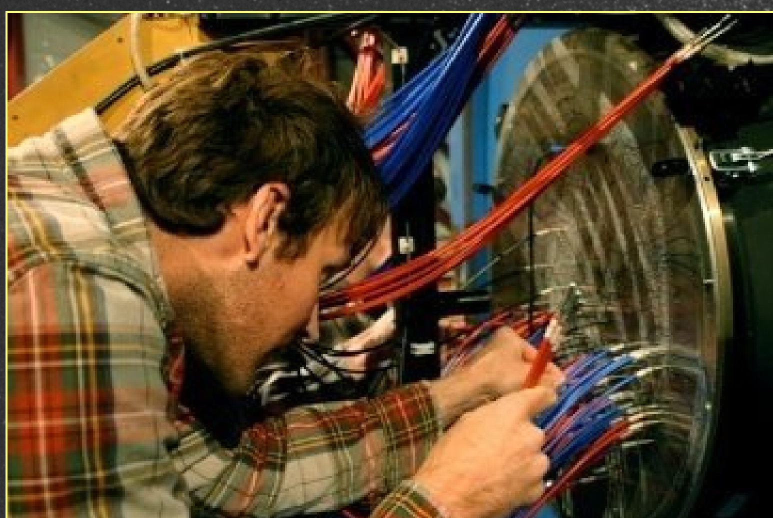

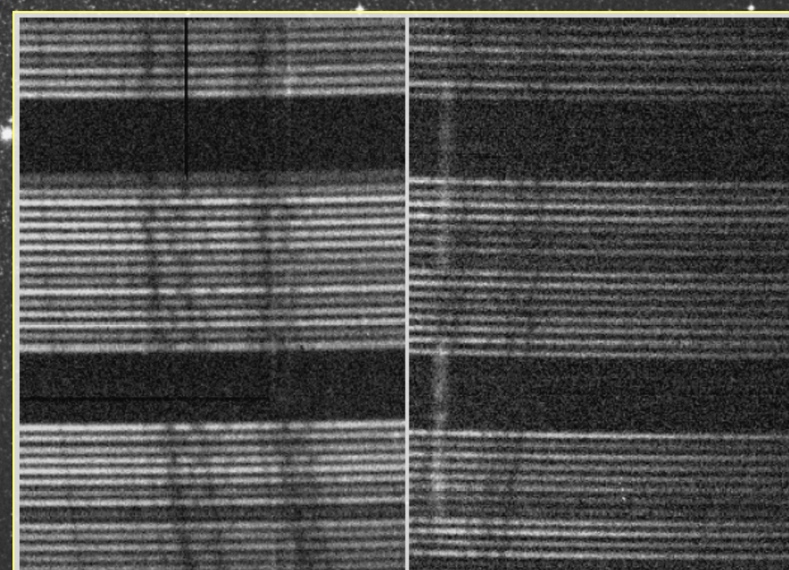

Data: Magellan Samples

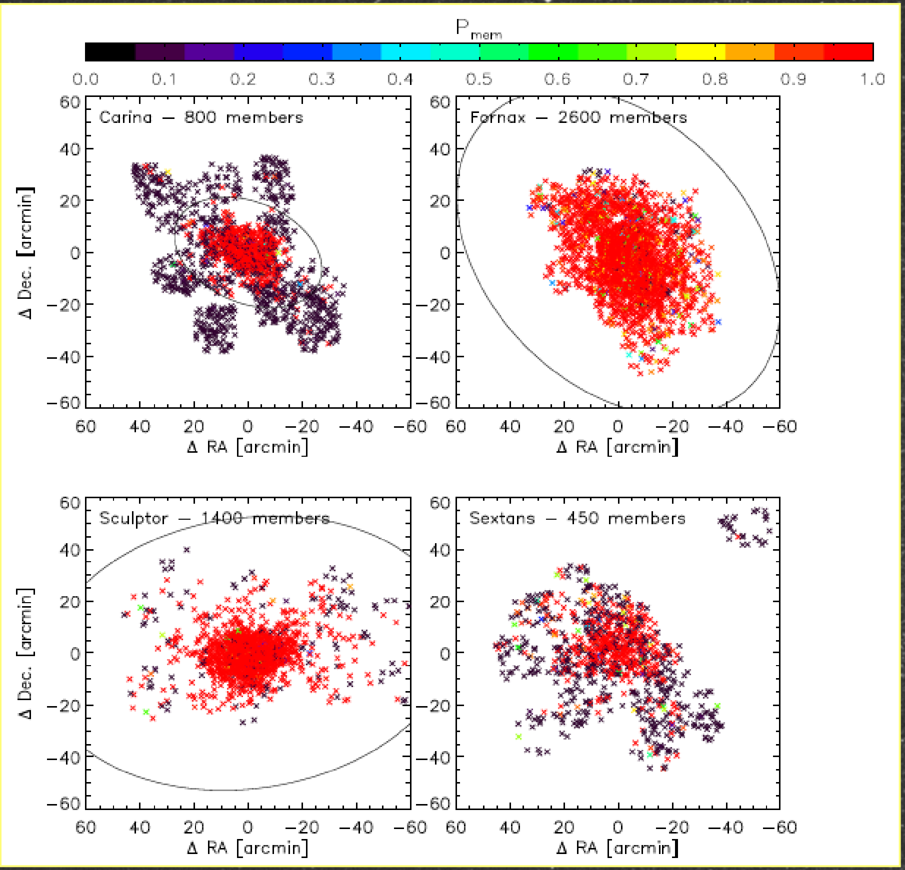

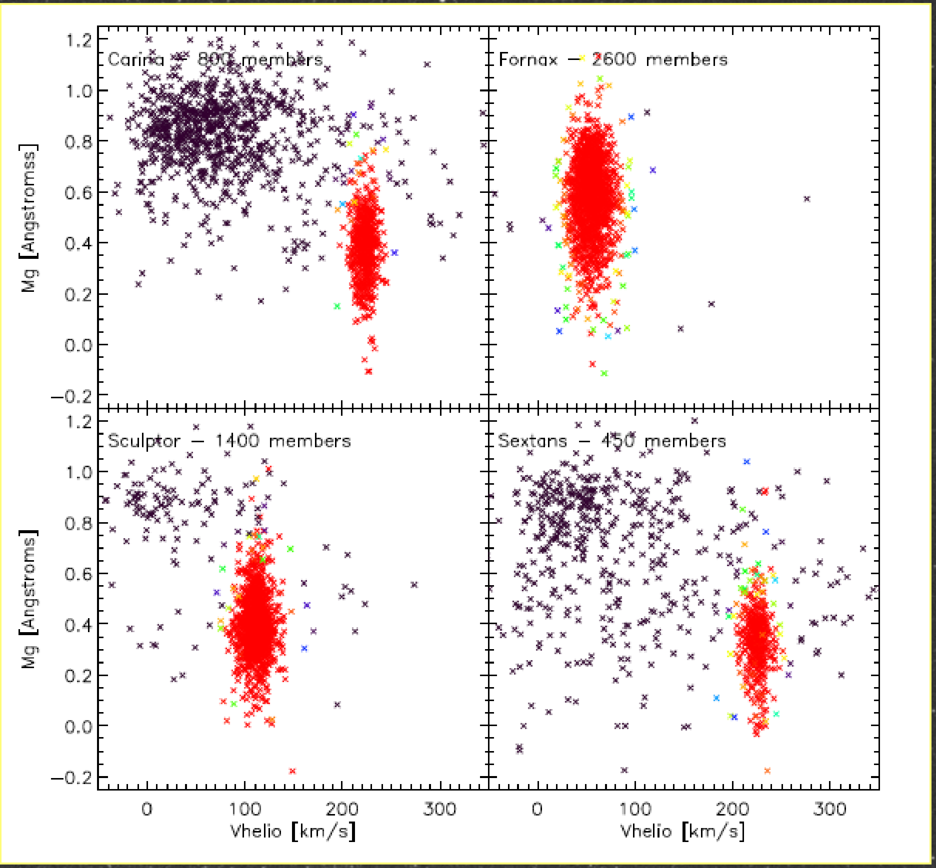

Walker etal (2009)

Velocity Dispersion Profiles for 'Classical' dSphs

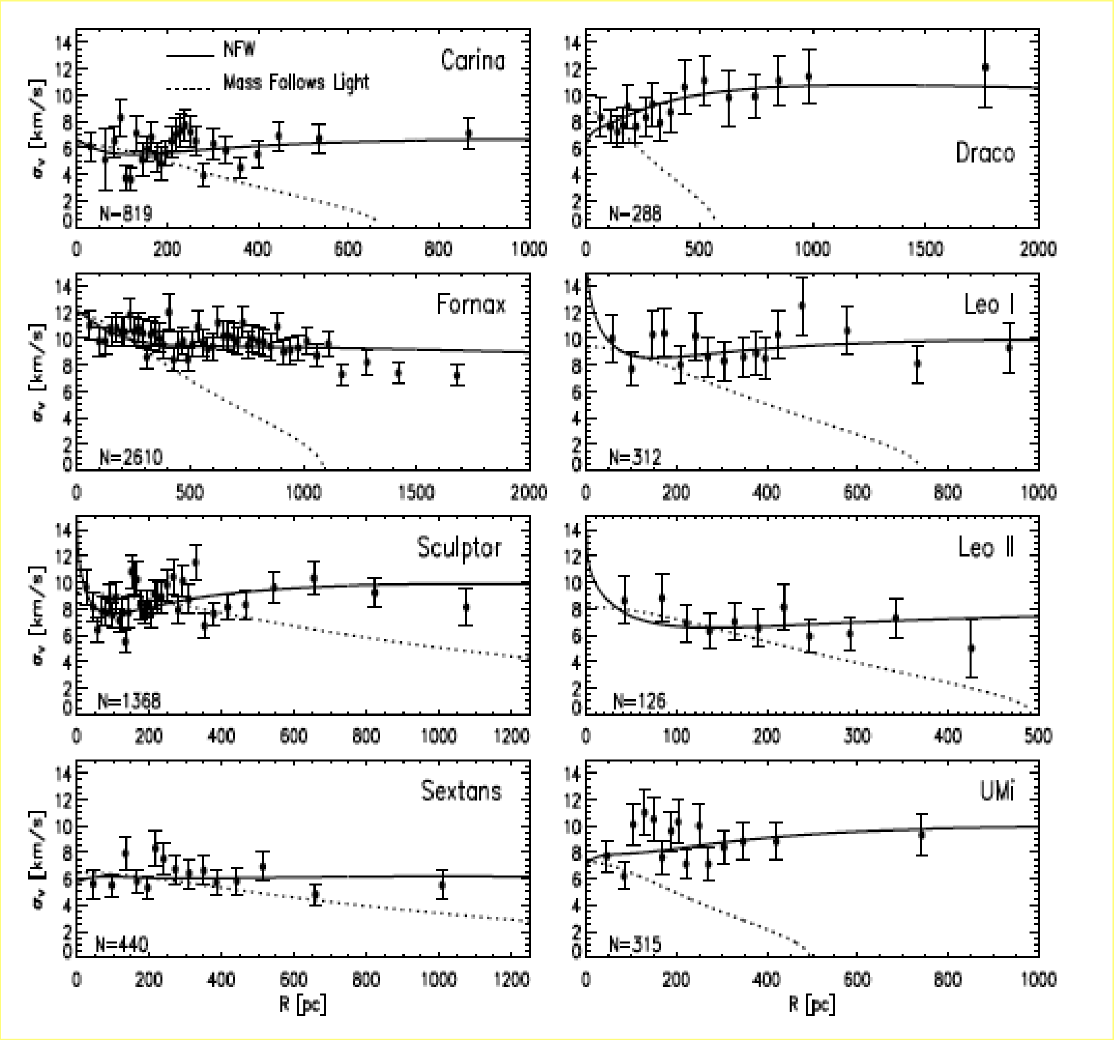

Walker etal. 2009

Kinematics with the Jeans Equation

Assumptions: Spherical symmetry, Dynamical equilibrium, negligible binary motions

1) Collisionless Boltzmann Eq.

$$\frac{\partial f}{\partial t} + \mathbf{v}.\frac{\partial f}{\partial \mathbf{r}} - \nabla\Phi.\frac{\partial f}{\partial \mathbf{v}} = 0$$

2) Jeans Eq. (spherical)

$$\frac{1}{\nu}\frac{d}{dr}(\nu \bar{v_r^2}) + 2\frac{\beta \bar{v_r^2}}{r} = -\frac{GM(r)}{r^2}$$

3) Solution in terms of observables

$$\sigma_p^2(R) = \frac{2}{I(R)}\int_R^\infty \left(1 - \beta\frac{R^2}{r^2}\right)\frac{\nu(r)\bar{v_r^2}r}{\sqrt{r^2 - R^2}}dr$$

4) Adopt Halo Model

$$\rho(r) = \rho_0\left(\frac{r}{r_0}\right)^{-\gamma}\left[1 + \left(\frac{r}{r_0}\right)^{\alpha}\right]^{\frac{\gamma-\eta}{\alpha}}$$

$\gamma = 0$ --> Core

$\gamma = \alpha = 1$ --> NFW Cusp

Kinematics with the Jeans Equation

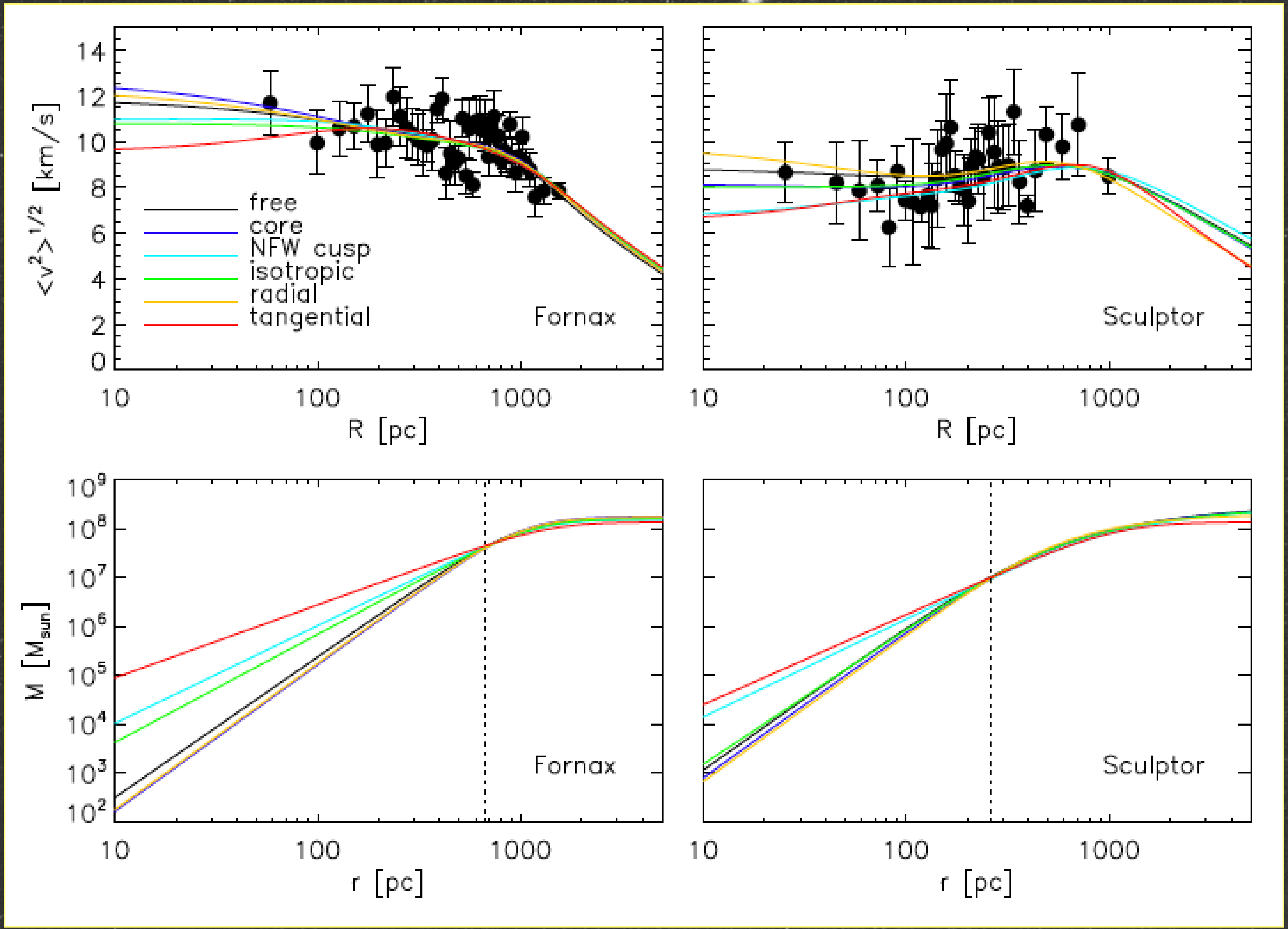

Simple Mass Estimates

Jeans Eq.

$$\frac{1}{\nu}\frac{d}{dr}(\nu\bar{v}_r^2) + 2\frac{\beta\bar{v}_r^2}{r} = -\frac{GM(r)}{r^2}$$

Isotropy, flat vdisp profile
(Plummer light profile) -->

$$M(r) = -\frac{r^2\bar{v}_r^2}{G\nu}\frac{d\nu}{dr} = \frac{5r_{half}\sigma^2\left(\frac{r}{r_{half}}\right)^3}{G[1 + r^2/r_{half}^2]}$$

$$\longrightarrow \quad M(R_{half}) \sim 5\sigma_V^2\frac{R_{half}}{2G}$$

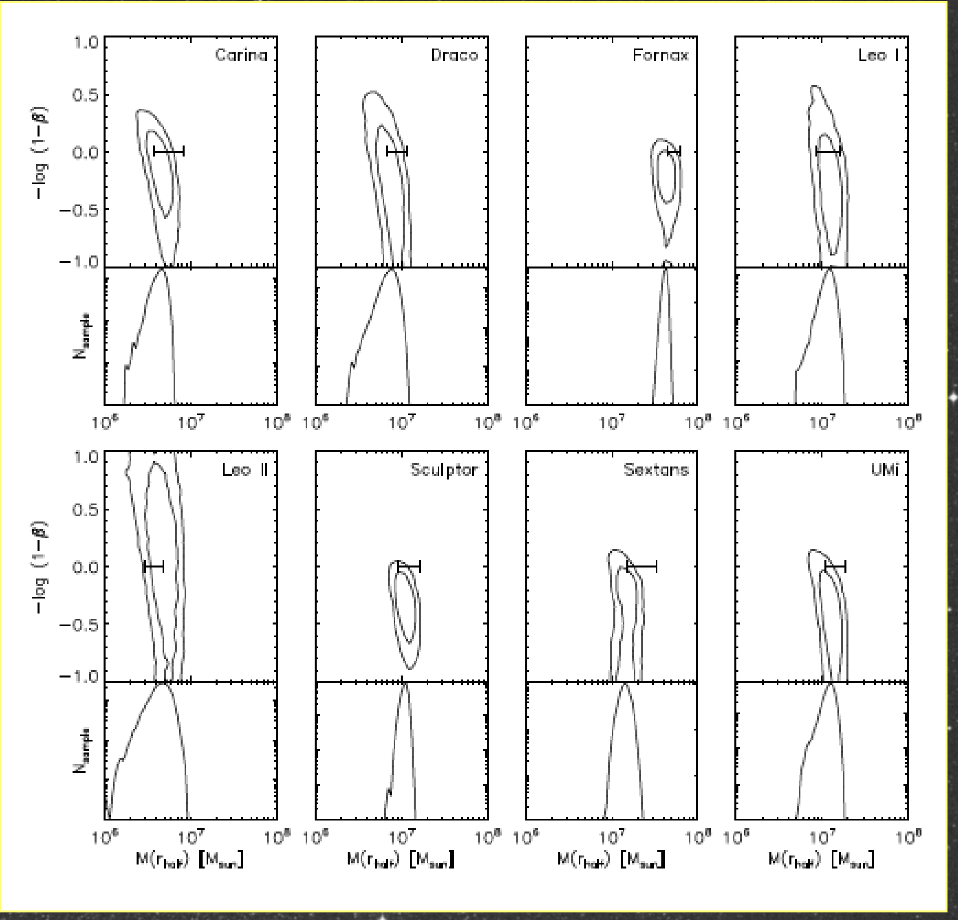

Walker et al. (2009), see also Peñarrubia et al. (2008), Wolf et al. (2010), Amorisco etal. (2010)

‘Retro’ Mass Estimates

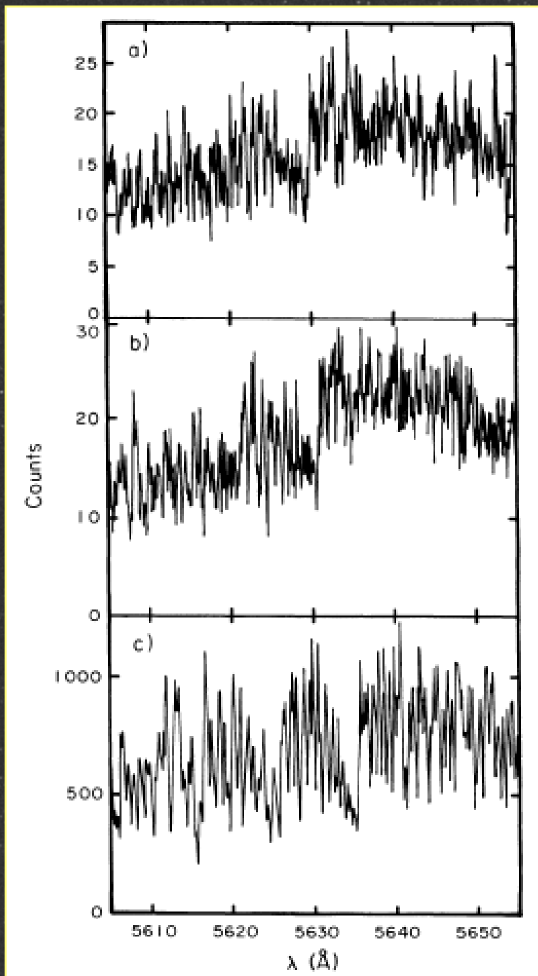

Aaronson (1983)

$$\sigma_V^2 \sim \frac{GM}{R}$$

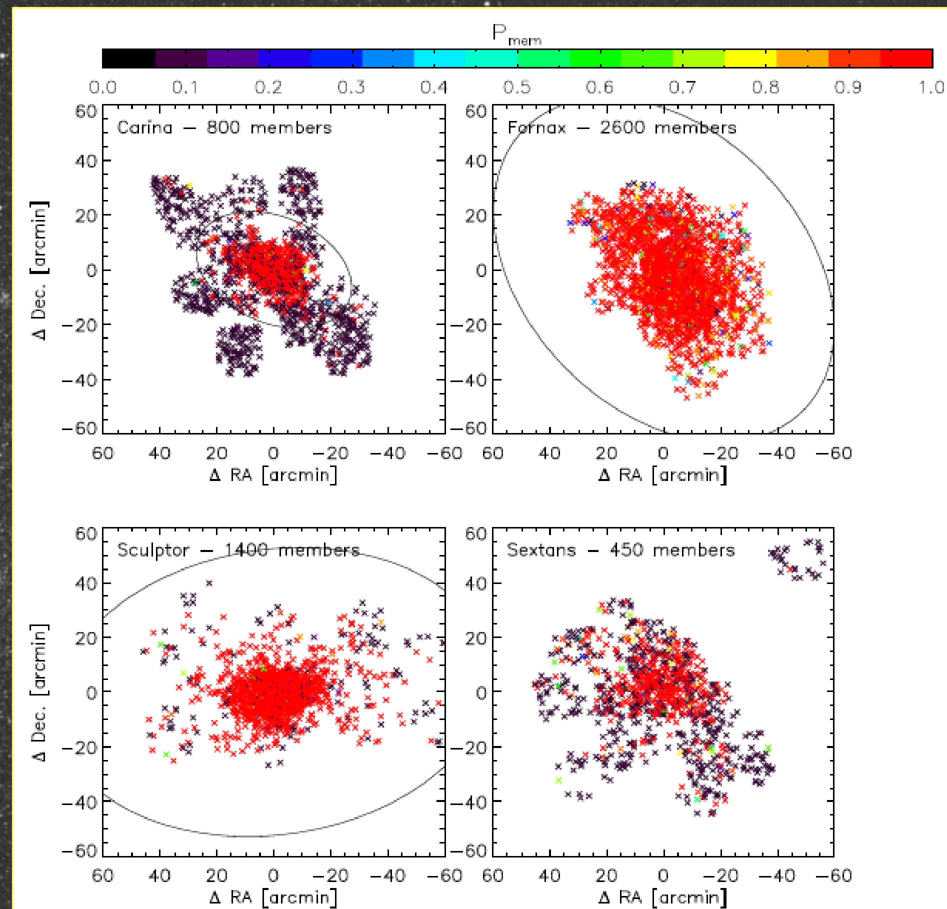

Stellar Dynamics

e.g., Wilkinson et al. (2002); -- Distribution Function Modeling

Chanamé et al. (2008); -- Schwarzschild Modeling

talks here by Mark Wilkinson, Gary Mamon, Joe Wolf (and quite possibly others)

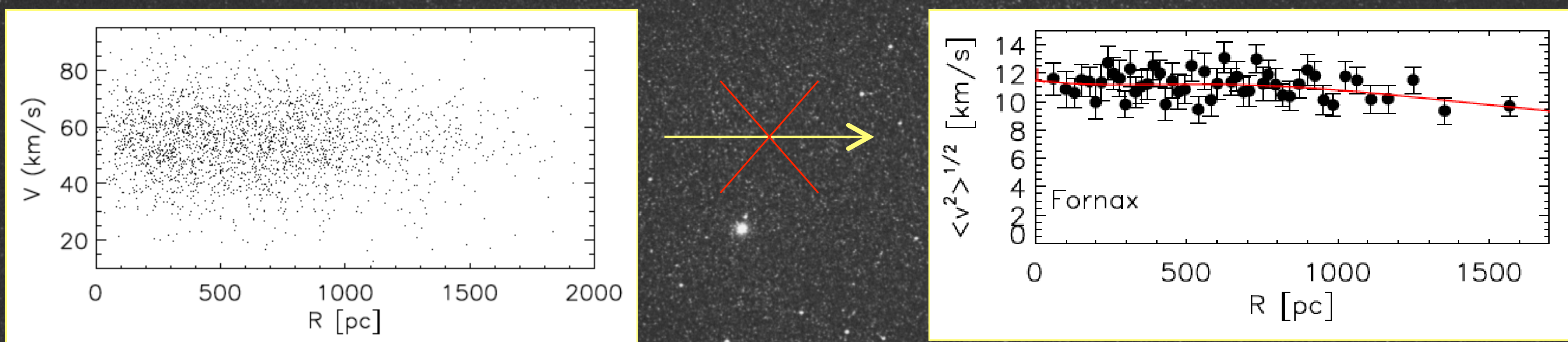

Cores vs cusps

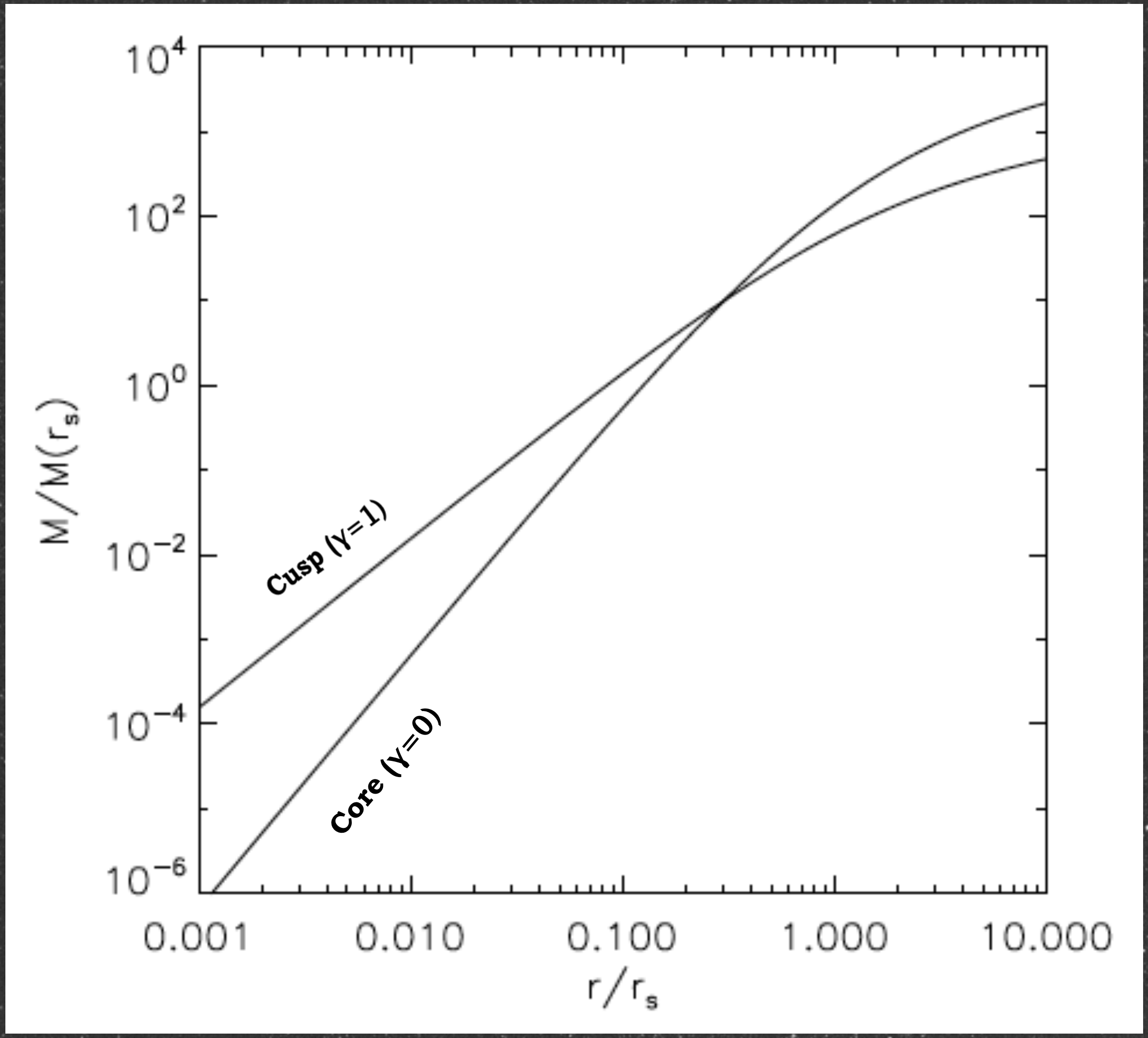

$$M(r_h) \approx \frac{5 r_h \sigma_V^2}{2G}$$

Two distinct ancient components in the Sculptor Dwarf Spheroidal Galaxy: First Results from DART[1]

Eline Tolstoy[2], M.J. Irwin[3], A. Helmi[2], G. Battaglia[2], P. Jablonka[4], V. Hill[4], K.A. Venn[5], M.D. Shetrone[6], B. Letarte[2], A.A. Cole[2], F. Primas[7], P. Francois[4], N. Arimoto[8], K. Sadakane[8], A. Kaufer[9], T. Szeifert[9], T. Abel[10],

ABSTRACT

We have found evidence for the presence of two distinct ancient stellar components (both $\geq$ 10 Gyr old) in the Sculptor dwarf spheroidal galaxy. We used the ESO Wide Field Imager (WFI) in conjunction with the VLT/FLAMES spectrograph to study the properties of the resolved stellar population of Sculptor out to and beyond the tidal radius. We find that two components are discernible in the spatial distribution of Horizontal Branch stars in our imaging, and in the [Fe/H] and v_{hel} distributions for our large sample of spectroscopic measurements. They can be generally described as a "metal-poor" component ([Fe/H]< -1.7) and a "metal-rich" component ([Fe/H]> -1.7). The metal-poor stars are more spatially extended than the metal-rich stars, and they also appear to be kinematically distinct. These results provide an important insight into the formation processes of small systems in the early universe and the conditions found there. Even this simplest of galaxies appears to have had a surprisingly complex early evolution.

Also:
Fornax (Battaglia et al. 2006)
Sextans: (Battaglia et al. 2010)

$$M(r_h) \approx \frac{5 r_h \sigma_V^2}{2G}$$

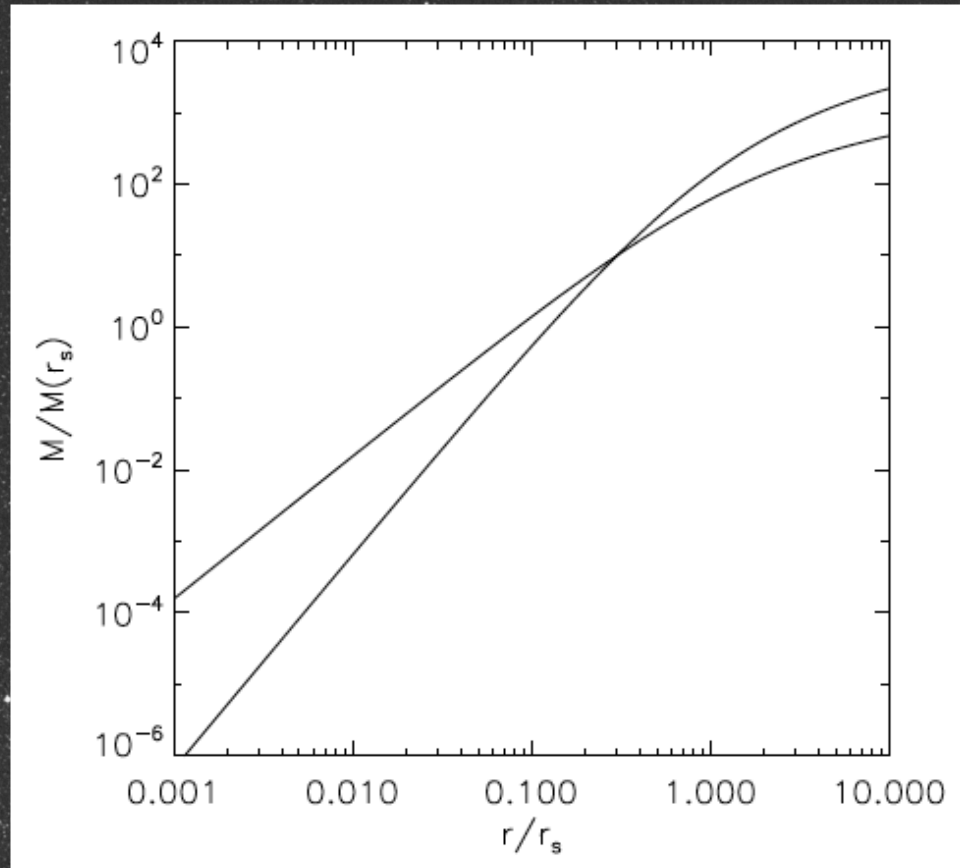

$$\Gamma \equiv \frac{\Delta \log M}{\Delta \log r} = \frac{\log[M(r_{\mathrm{h},2})/M(r_{\mathrm{h},1})]}{\log[r_{\mathrm{h},2}/r_{\mathrm{h},1}]} \approx 1 + \frac{\log[\sigma_{V,2}^2/\sigma_{V,1}^2]}{\log[r_{\mathrm{h},2}/r_{\mathrm{h},1}]}$$

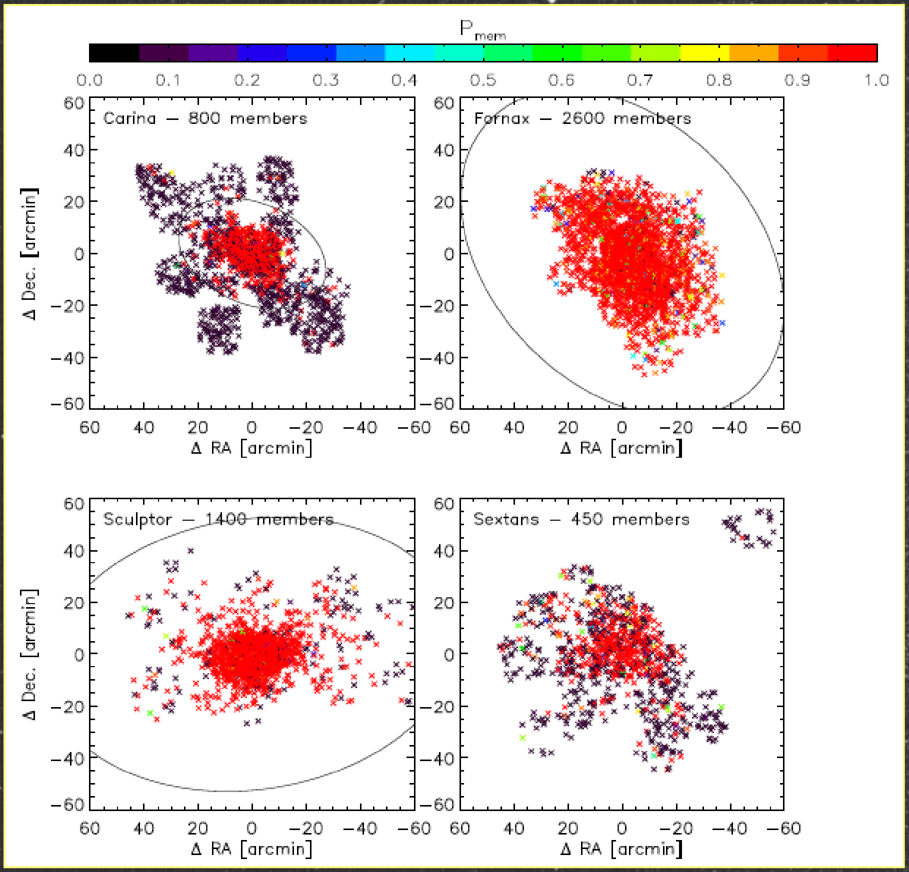

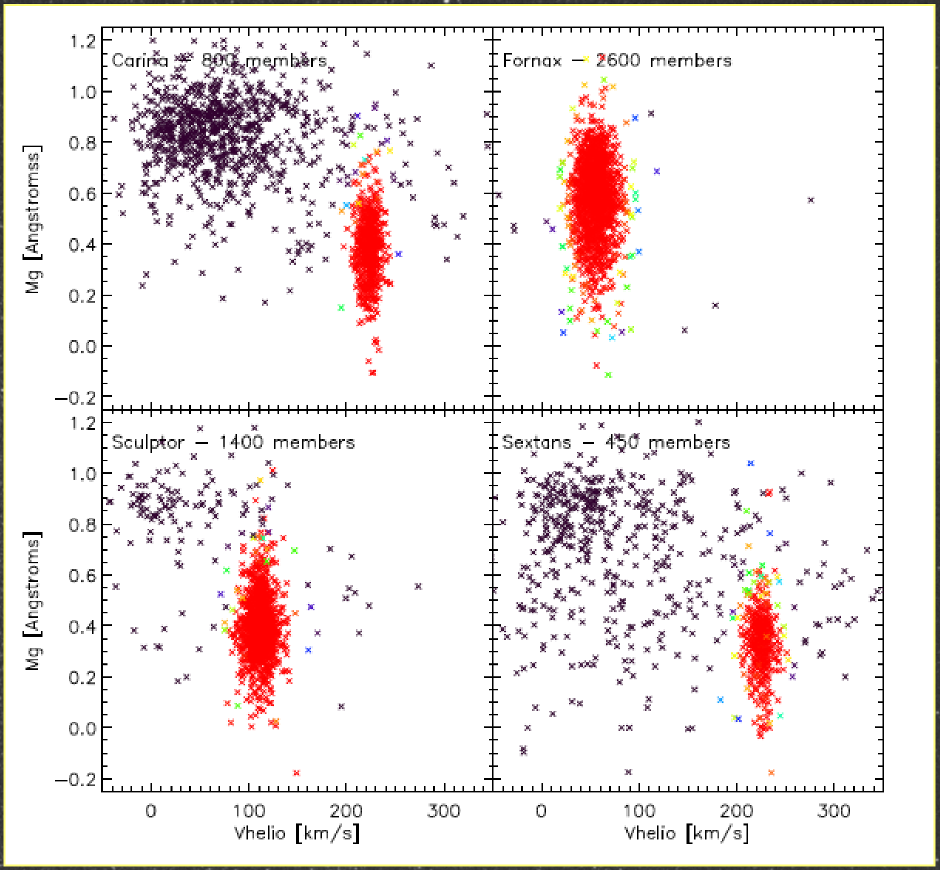

Walker etal (2009)

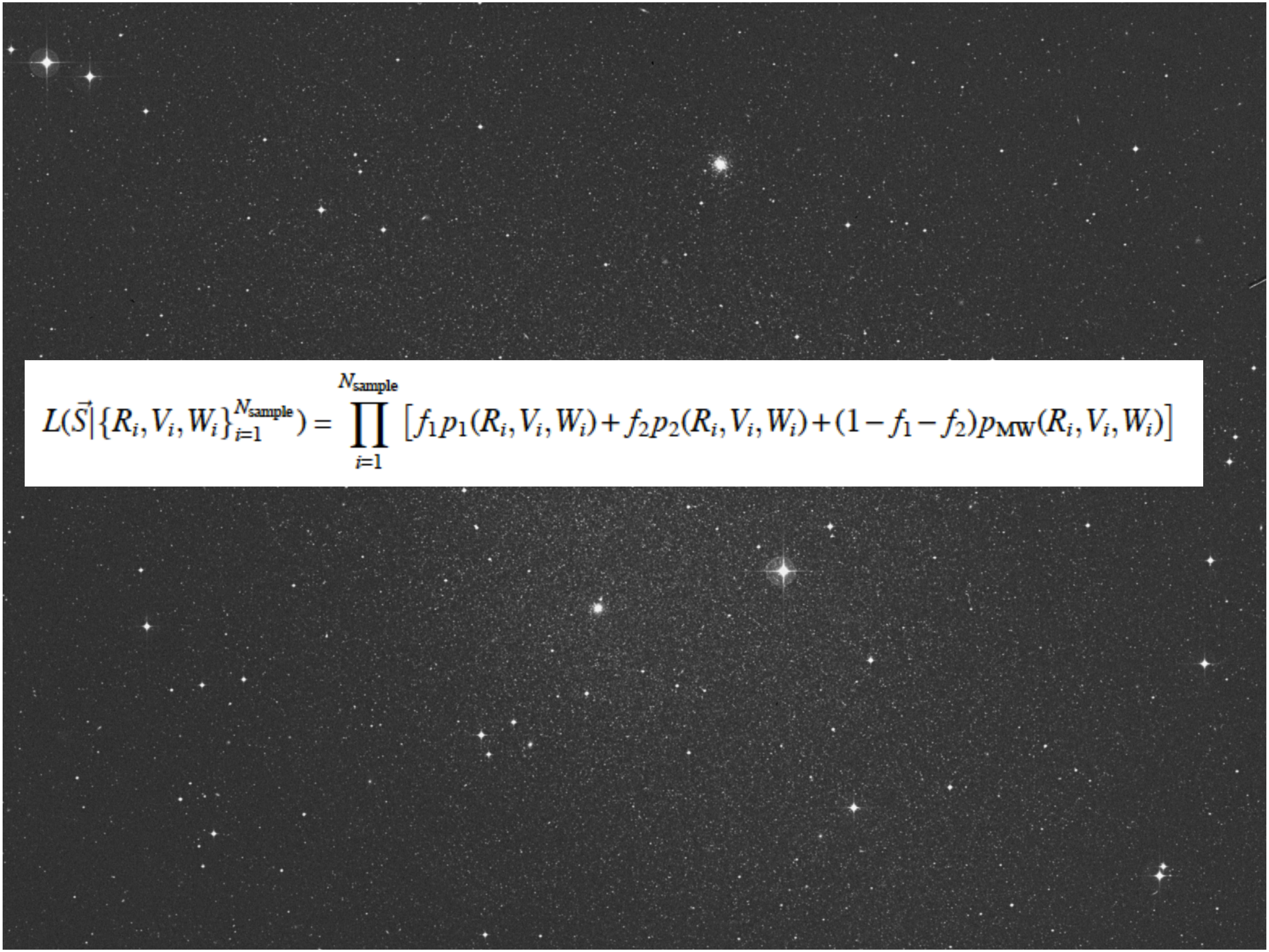

$$L(\vec{S}|\{R_i, V_i, W_i\}_{i=1}^{N_{\rm sample}}) = \prod_{i=1}^{N_{\rm sample}} \left[f_1 p_1(R_i, V_i, W_i) + f_2 p_2(R_i, V_i, W_i) + (1 - f_1 - f_2) p_{\rm MW}(R_i, V_i, W_i) \right]$$

$$p_1(R_i,V_i,W_i) = p_{V,1}(V_i)p_{W,1}(W_i)\frac{\theta(R_i)p_{R,1}(R_i)}{\int_0^\infty \theta(R)p_{R,1}(R)dR};$$

$$p_2(R_i,V_i,W_i) = p_{V,2}(V_i)p_{W,2}(W_i)\frac{\theta(R_i)p_{R,2}(R_i)}{\int_0^\infty \theta(R)p_{R,2}(R)dR};$$

$$p_{\mathrm{MW}}(R_i,V_i,W_i) = \hat{p}_{V,\mathrm{MW}}(V_i)\hat{p}_{W,\mathrm{MW}}(W_i)\hat{p}_{R,\mathrm{MW}}(R_i)$$

$$p_{R,1}(R) = \frac{2R/r_{h,1}^2}{\left(1+R^2/r_{h,1}^2\right)^2}$$

$$p_{V,1}(V,\alpha_*,\delta_*) = \frac{1}{\sqrt{2\pi(\sigma_{V,1}^2+\epsilon_V^2)}}\exp\left[-\frac{1}{2}\frac{(V-\langle V\rangle_{\alpha_*,\delta_*})^2}{\sigma_{V,1}^2+\epsilon_V^2}\right]$$

$$p_{W,1}(W) = \frac{1}{\sqrt{2\pi(\sigma_{W,1}^2+\epsilon_W^2)}}\exp\left[-\frac{1}{2}\frac{(W-\langle W\rangle_1)^2}{\sigma_{W,1}^2+\epsilon_W^2}\right]$$

$$p_1(R_i, V_i, W_i) = p_{V,1}(V_i)\, p_{W,1}(W_i) \frac{\theta(R_i)\, p_{R,1}(R_i)}{\displaystyle\int_0^\infty \theta(R)\, p_{R,1}(R)\, dR};$$

$$p_2(R_i, V_i, W_i) = p_{V,2}(V_i)\, p_{W,2}(W_i) \frac{\theta(R_i)\, p_{R,2}(R_i)}{\displaystyle\int_0^\infty \theta(R)\, p_{R,2}(R)\, dR};$$

$$p_{\mathrm{MW}}(R_i, V_i, W_i) = \hat{p}_{V,\mathrm{MW}}(V_i)\, \hat{p}_{W,\mathrm{MW}}(W_i)\, \hat{p}_{R,\mathrm{MW}}(R_i)$$

$$\hat{p}_{R,\mathrm{MW}}(R) = \frac{1}{\displaystyle\sum_{i=1}^{N_{\mathrm{sample}}} (1 - P_{\mathrm{mem},i})} \sum_{i=1}^{N_{\mathrm{sample}}} \frac{1 - P_{\mathrm{mem},i}}{\sqrt{2\pi k^2}} \exp\left[-\frac{1}{2} \frac{(R_i - R)^2}{k^2} \right];$$

$$\hat{p}_{V,\mathrm{MW}}(V) = \frac{1}{\displaystyle\sum_{i=1}^{N_{\mathrm{sample}}} (1 - P_{\mathrm{mem},i})} \sum_{i=1}^{N_{\mathrm{sample}}} \frac{1 - P_{\mathrm{mem},i}}{\sqrt{2\pi \epsilon_{V,i}^2}} \exp\left[-\frac{1}{2} \frac{(V_i - V)^2}{\epsilon_{V,i}^2} \right];$$

$$\hat{p}_{W,\mathrm{MW}}(W) = \frac{1}{\displaystyle\sum_{i=1}^{N_{\mathrm{sample}}} (1 - P_{\mathrm{mem},i})} \sum_{i=1}^{N_{\mathrm{sample}}} \frac{1 - P_{\mathrm{mem},i}}{\sqrt{2\pi \epsilon_{W,i}^2}} \exp\left[-\frac{1}{2} \frac{(W_i - W)^2}{\epsilon_{W,i}^2} \right],$$

$$L(\vec{S}|\{R_i, V_i, W_i\}_{i=1}^{N_{\mathrm{sample}}}) = \prod_{i=1}^{N_{\mathrm{sample}}} \left[f_1 p_1(R_i, V_i, W_i) + f_2 p_2(R_i, V_i, W_i) + (1 - f_1 - f_2) p_{\mathrm{MW}}(R_i, V_i, W_i) \right]$$

MCMC Parameters and Top-Hat Priors for Two-Component Model

Parameter	Minimum	Maxium	Description
f_{mem}	0	1	$\equiv (N_1 + N_2)/(N_1 + N_2 + N_{\mathrm{MW}})$, fraction of stars belonging to dSph
f_{sub}	0	1	$\equiv N_1/(N_1 + N_2)$, fraction of members belonging to MR component
$r_{h,1}/r_{h,2}$	0	1	ratio of half-light radii for metal-rich (MR) and metal-poor (MP) components
$\log_{10}[r_{h,2}/\mathrm{pc}]$	0	3	half-light radius of MP component
$\langle W \rangle_1/\mathrm{Å}$	−3	+3	mean reduced Mg index of MR component
$(\langle W \rangle_1 - \langle W \rangle_2)/\mathrm{Å}$	0	3	offset of mean Mg indices
$\log_{10}[\sigma^2_{W,1}/\mathrm{Å}^2]$	−5	+1	squared dispersion of reduced Mg index, MR component
$\log_{10}[\sigma^2_{W,2}/\mathrm{Å}^2]$	−5	+1	squared dispersion of reduced Mg index, MP component
$\log_{10}[\sigma^2_{V,1}/(\mathrm{km}^2\mathrm{s}^{-2})]$	−5	+5	squared velocity dispersion, MR component
$\log_{10}[\sigma^2_{V,2}/(\mathrm{km}^2\mathrm{s}^{-2})]$	−5	+5	squared velocity dispersion, MP component
$\mu_\alpha/(\mathrm{mas/century})$	−1000	+1000	RA proper motion of dSph
$\mu_\delta/(\mathrm{mas/century})$	−1000	+1000	Dec. proper motion of dSph

TESTS ON SYNTHETIC DATA: INPUT PARAMETERS FOR DYNAMICAL TEST MODELS

Stellar Profile (Equation 14)					Dark Matter Profile (Equation 15)				
β_{ani}	r_* [pc]	α_*	β_*	γ_*	ρ_{DM} [$M_\odot$pc^{-3}]	r_{DM} [pc]	α_{DM}	β_{DM}	γ_{DM}
Cored Halos									
Isotropic									
0.00	100	2	5	0.0	0.064	1000	2	3.1	0.0
0.00	250	2	5	0.0	0.064	1000	2	3.1	0.0
0.00	500	2	5	0.0	0.064	1000	2	3.1	0.0
0.00	1000	2	5	0.0	0.064	1000	2	3.1	0.0
Radially Anisotropic									
+0.25	100	2	5	0.6	0.064	1000	2	3.1	0.0
+0.25	250	2	5	0.6	0.064	1000	2	3.1	0.0
+0.25	500	2	5	0.6	0.064	1000	2	3.1	0.0
+0.25	1000	2	5	0.6	0.064	1000	2	3.1	0.0
Tangentially Anisotropic									
–0.45	100	2	5	0.0	0.064	1000	2	3.1	0.0
–0.45	250	2	5	0.0	0.064	1000	2	3.1	0.0
–0.45	500	2	5	0.0	0.064	1000	2	3.1	0.0
–0.45	1000	2	5	0.0	0.064	1000	2	3.1	0.0
Cusped Halos									
Isotropic									
0.00	100	2	5	0.1	0.014	1000	2	3.1	0.9
0.00	250	2	5	0.1	0.014	1000	2	3.1	0.9
0.00	500	2	5	0.1	0.014	1000	2	3.1	0.9
0.00	1000	2	5	0.1	0.014	1000	2	3.1	0.9
Radially Anisotropic									
+0.25	100	2	5	0.6	0.014	1000	2	3.1	0.9
+0.25	250	2	5	0.6	0.014	1000	2	3.1	0.9
+0.25	500	2	5	0.6	0.014	1000	2	3.1	0.9
+0.25	1000	2	5	0.6	0.014	1000	2	3.1	0.9
Tangentially Anisotropic									
–0.45	100	2	5	0.1	0.014	1000	2	3.1	0.9
–0.45	250	2	5	0.1	0.014	1000	2	3.1	0.9
–0.45	500	2	5	0.1	0.014	1000	2	3.1	0.9
–0.45	1000	2	5	0.1	0.014	1000	2	3.1	0.9

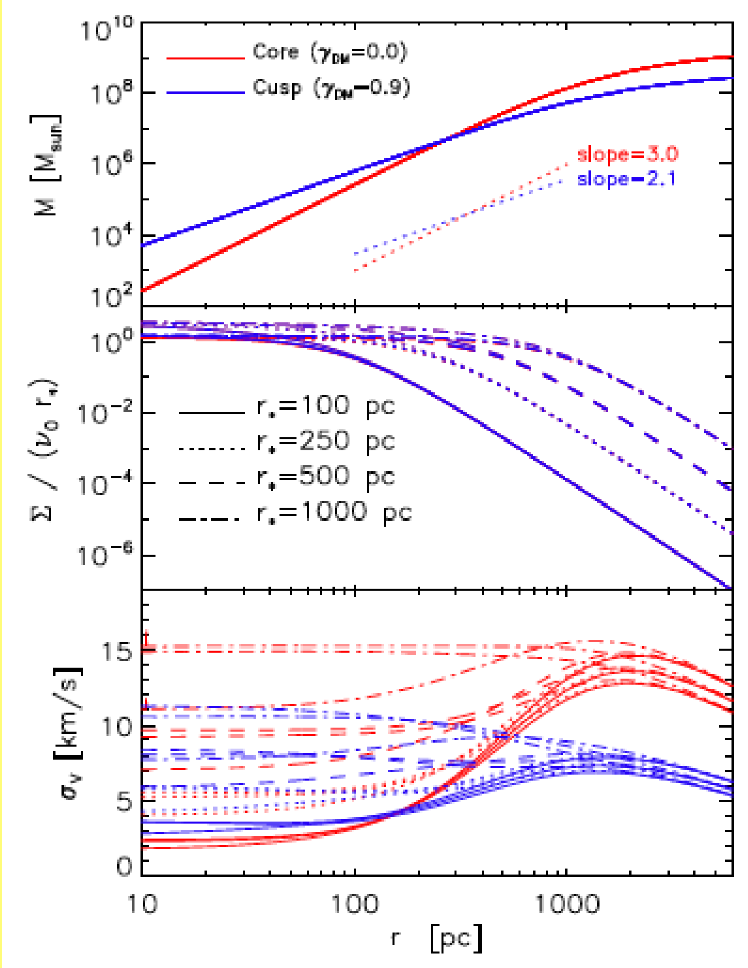

Models generated by Mark Wilkinson—for details see today's arxiv:1104.0412 (Charbonnier et al.)

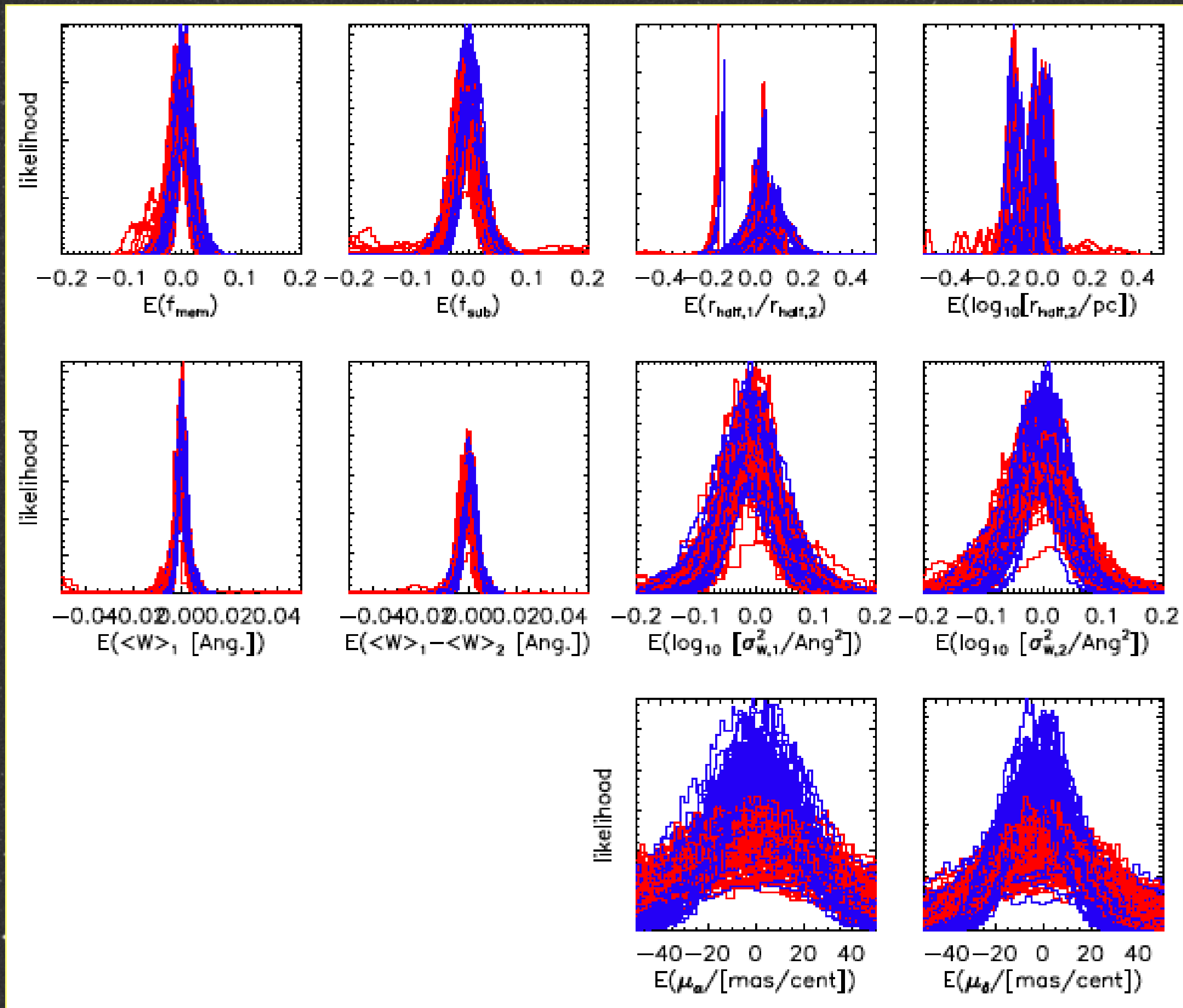
likelihood
−0.2 −0.1 0.0 0.1 0.2
E(f_mem)
−0.2 −0.1 0.0 0.1 0.2
E(f_sub)
−0.4−0.2 0.0 0.2 0.4
E(r_half,1/r_half,2)
−0.4−0.2 0.0 0.2 0.4
E(log10[r_half,2/pc])
likelihood
−0.040.020.000.020.04
E(<W>1 [Ang.])
−0.040.020.000.020.04
E(<W>1−<W>2 [Ang.])
−0.2 −0.1 0.0 0.1 0.2
E(log10 [σ²w,1/Ang²])
−0.2 −0.1 0.0 0.1 0.2
E(log10 [σ²w,2/Ang²])
likelihood
−40−20 0 20 40
E(μα/[mas/cent])
−40−20 0 20 40
E(μδ/[mas/cent])

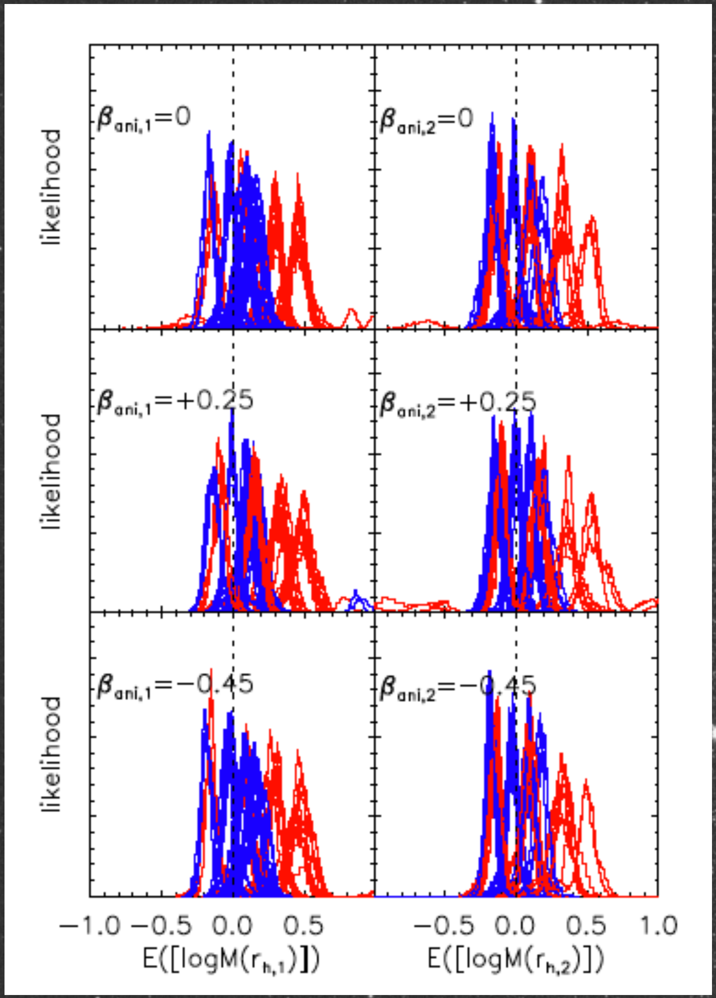

βani,1=0
βani,2=0
βani,1=+0.25
βani,2=+0.25
βani,1=−0.45
βani,2=−0.45
likelihood
−1.0 −0.5 0.0 0.5
−0.5 0.0 0.5 1.0
E([logM(rh,1)])
E([logM(rh,2)])

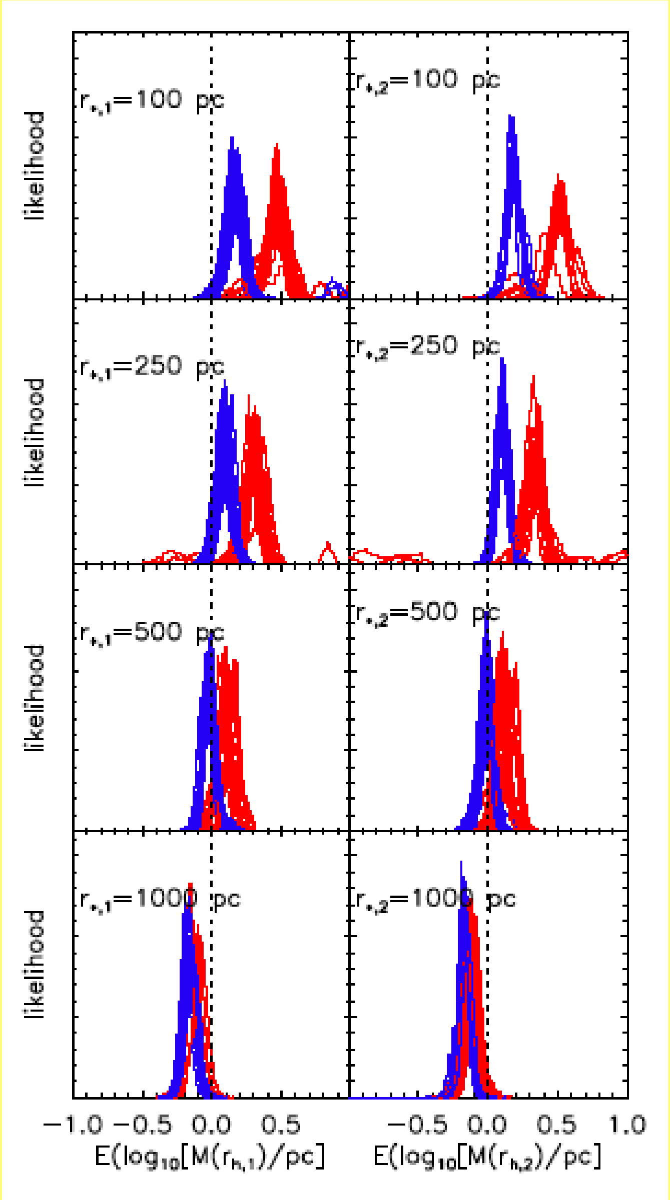

r*,1=100 pc
r*,2=100 pc
r*,1=250 pc
r*,2=250 pc
r*,1=500 pc
r*,2=500 pc
r*,1=1000 pc
r*,2=1000 pc
likelihood
−1.0 −0.5 0.0 0.5
−0.5 0.0 0.5 1.0
E(log10[M(rh,1)/pc]
E(log10[M(rh,2)/pc]

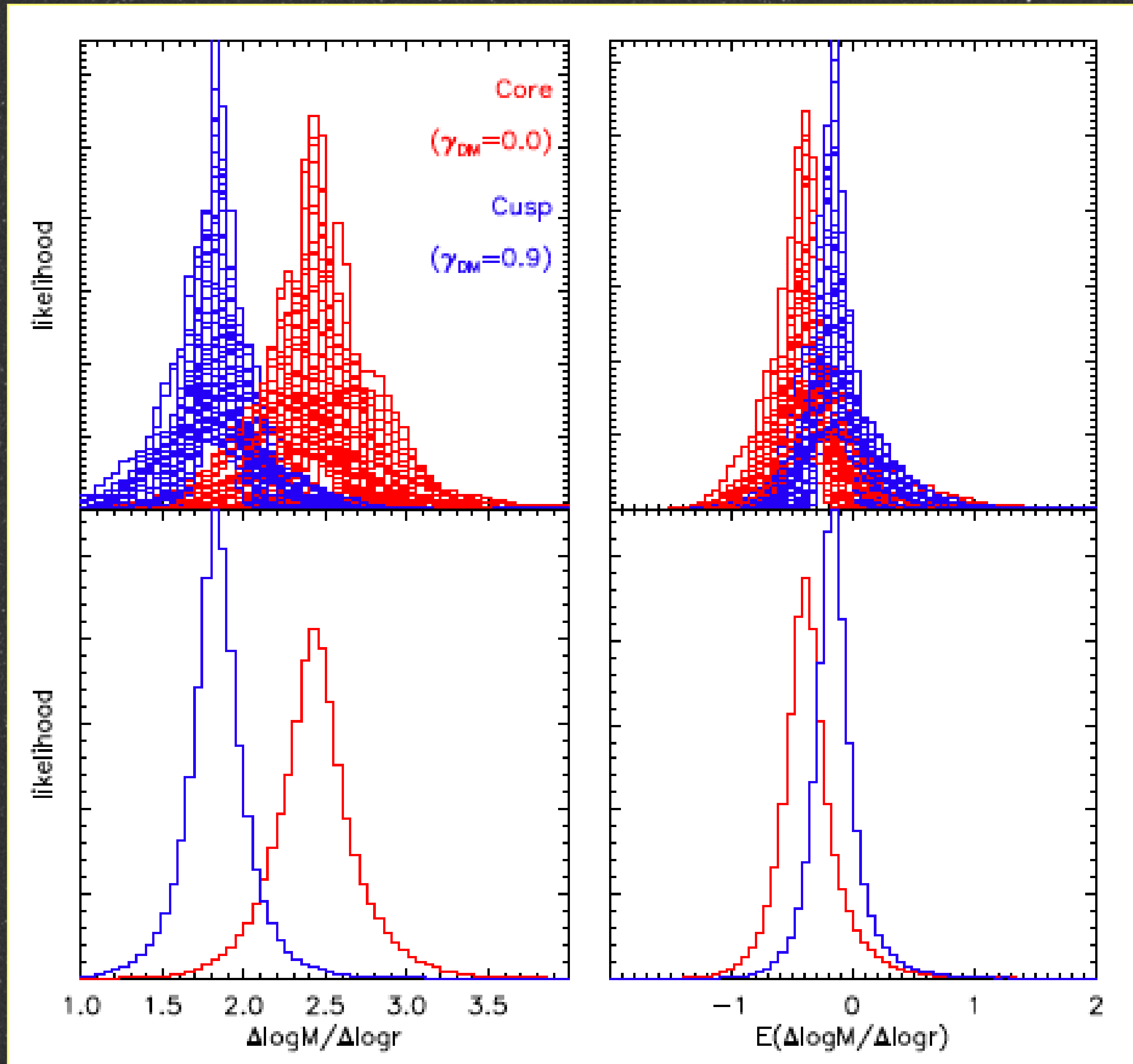
Core
(γ_{DM}=0.0)
Cusp
(γ_{DM}=0.9)
likelihood
likelihood
1.0
1.5
2.0
2.5
3.0
3.5
ΔlogM/Δlogr
−1
0
1
2
E(ΔlogM/Δlogr)

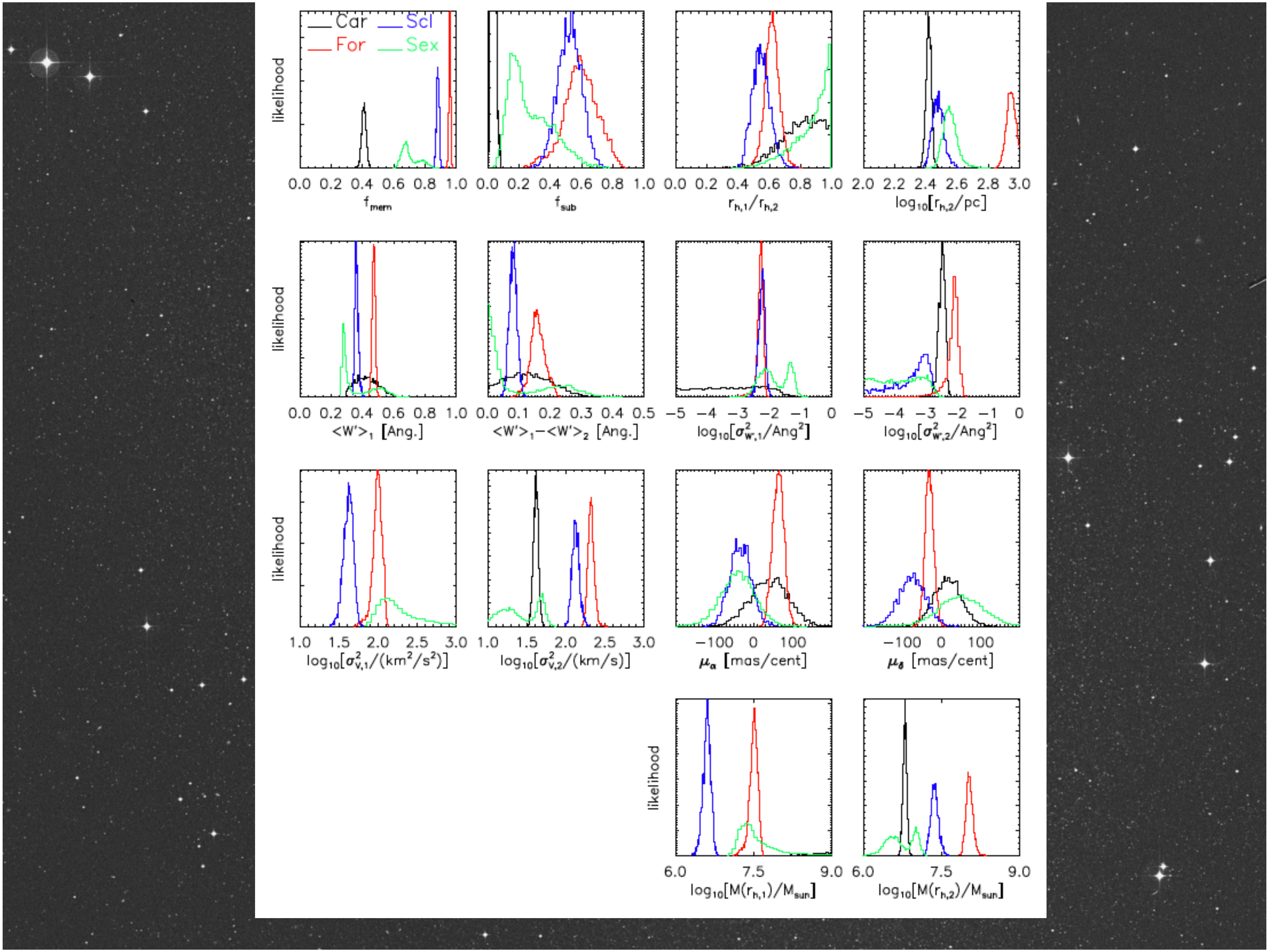
Car
Scl
For
Sex
likelihood
f_mem
f_sub
r_h,1/r_h,2
log10[r_h,2/pc]
<W'>_1 [Ang.]
<W'>_1−<W'>_2 [Ang.]
log10[σ²_W,1/Ang²]
log10[σ²_W,2/Ang²]
log10[σ²_V,1/(km²/s²)]
log10[σ²_V,2/(km/s)]
μ_α [mas/cent]
μ_δ [mas/cent]
log10[M(r_h,1)/M_sun]
log10[M(r_h,2)/M_sun]

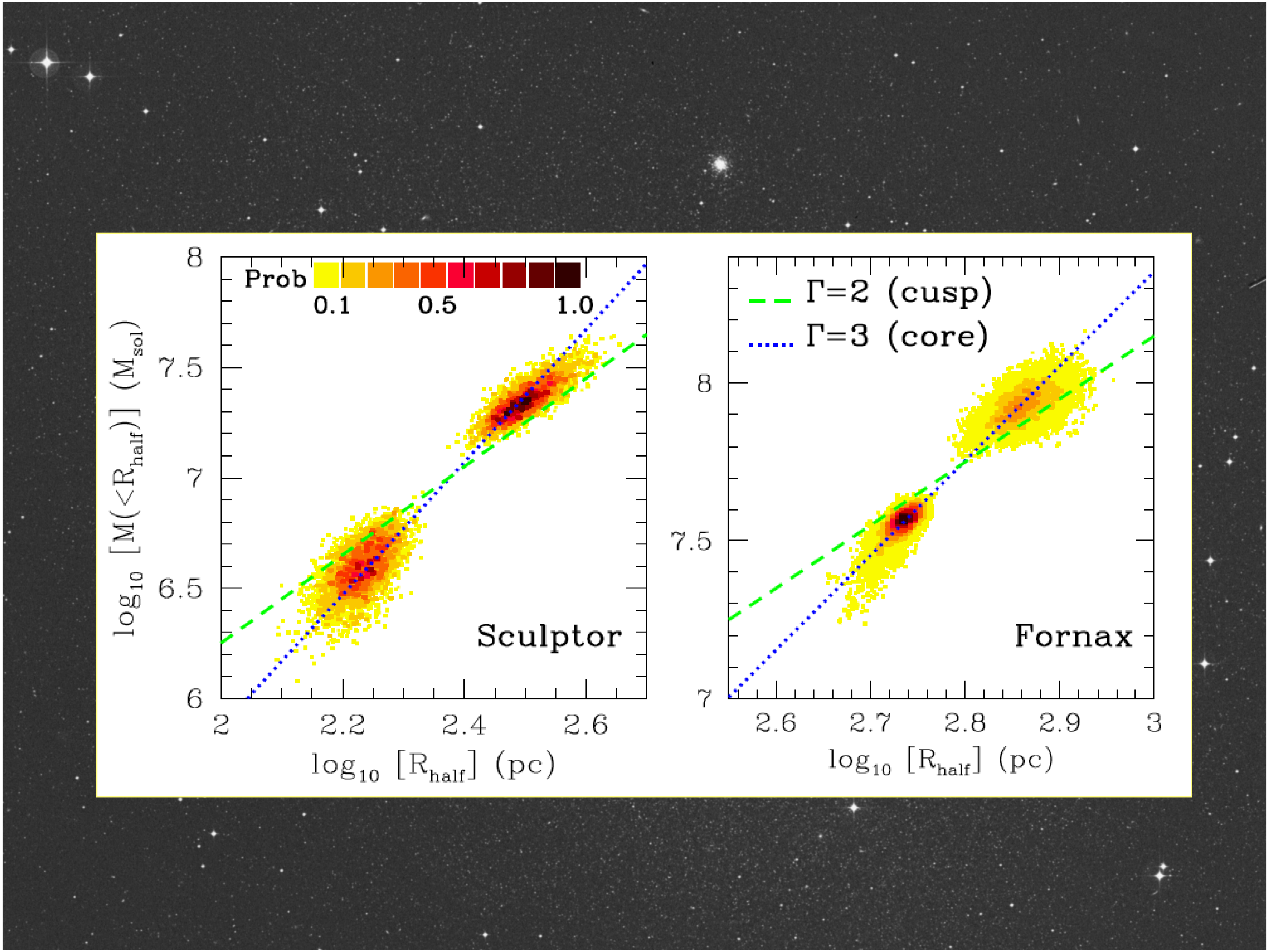

Prob
0.1
0.5
1.0
Γ=2 (cusp)
Γ=3 (core)
Sculptor
Fornax
log10 [M(<Rhalf)] (Msol)
log10 [Rhalf] (pc)
log10 [Rhalf] (pc)

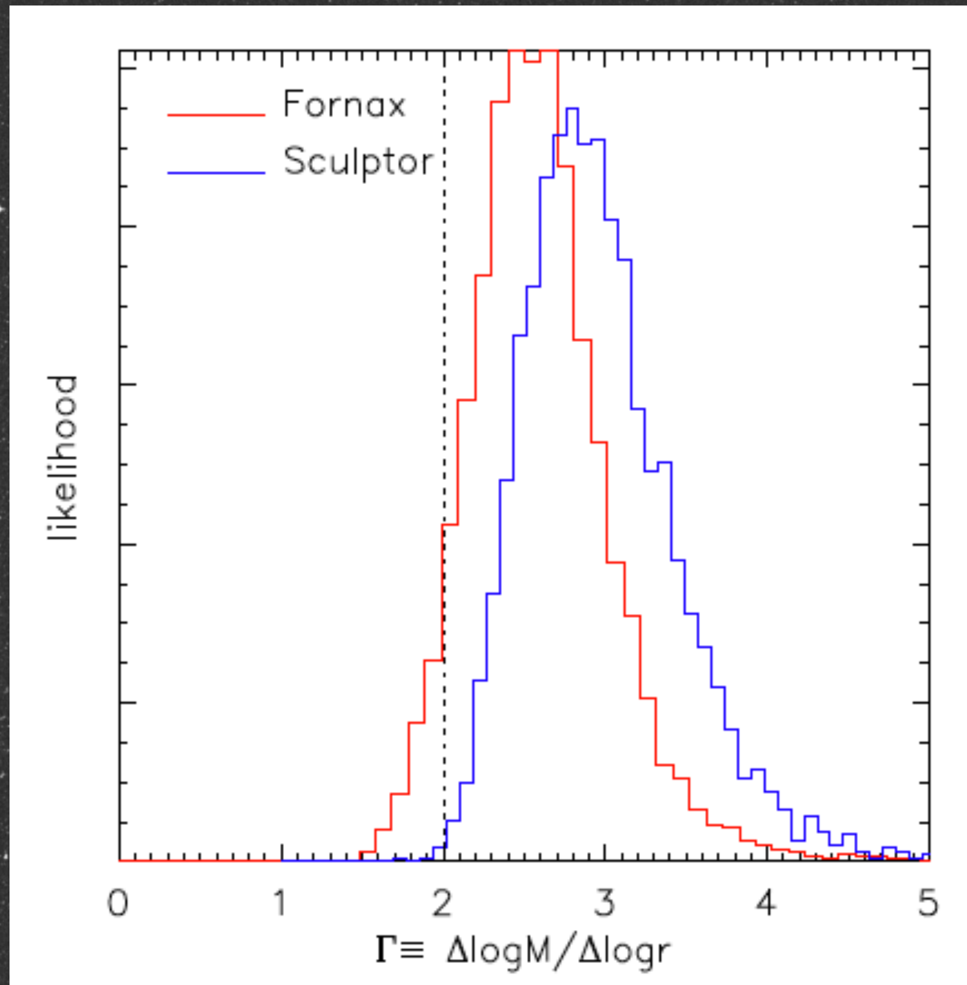

$$\Gamma \equiv \frac{\Delta \log M}{\Delta \log r} = \frac{\log[M(r_{\mathrm{h},2})/M(r_{\mathrm{h},1})]}{\log[r_{\mathrm{h},2}/r_{\mathrm{h},1}]} \approx 1 + \frac{\log[\sigma^2_{V,2}/\sigma^2_{V,1}]}{\log[r_{\mathrm{h},2}/r_{\mathrm{h},1}]}$$


END

Observations: Spectroscopy of "Classical" dSphs

$$CCF(v) = \int S(v)[T(v) - v]\, dv$$

$$W = \int_{\lambda 1}^{\lambda_2} [1 - S(\lambda)/C(\lambda)]\, d\lambda$$

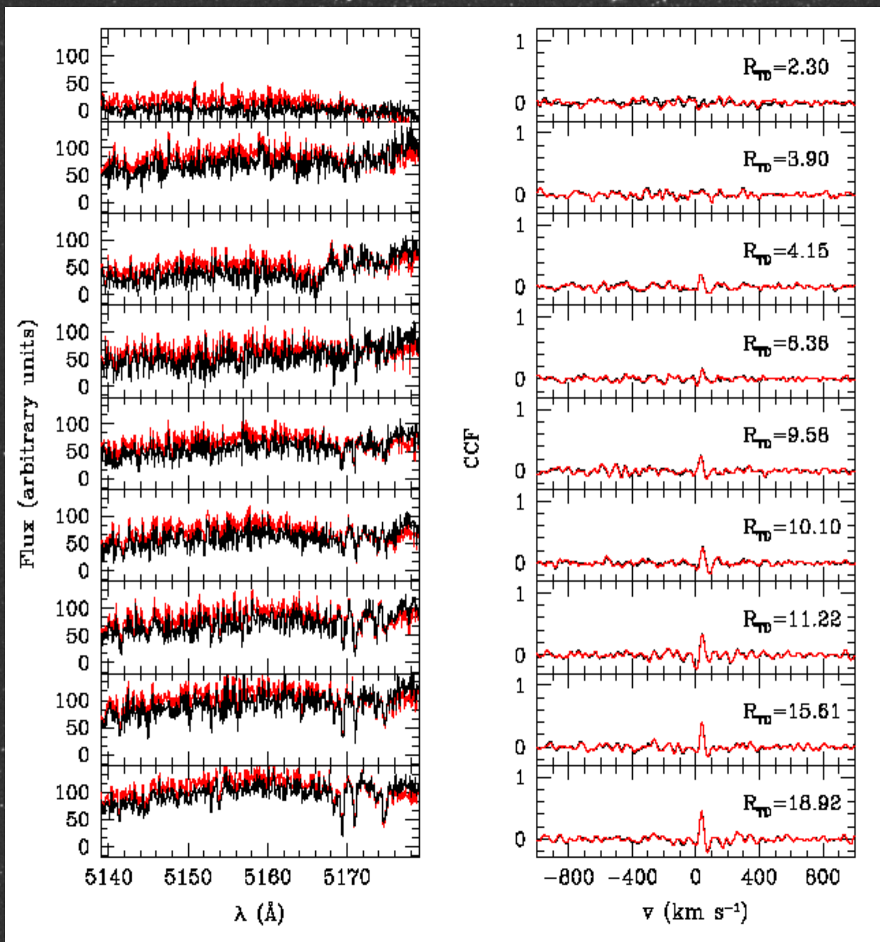

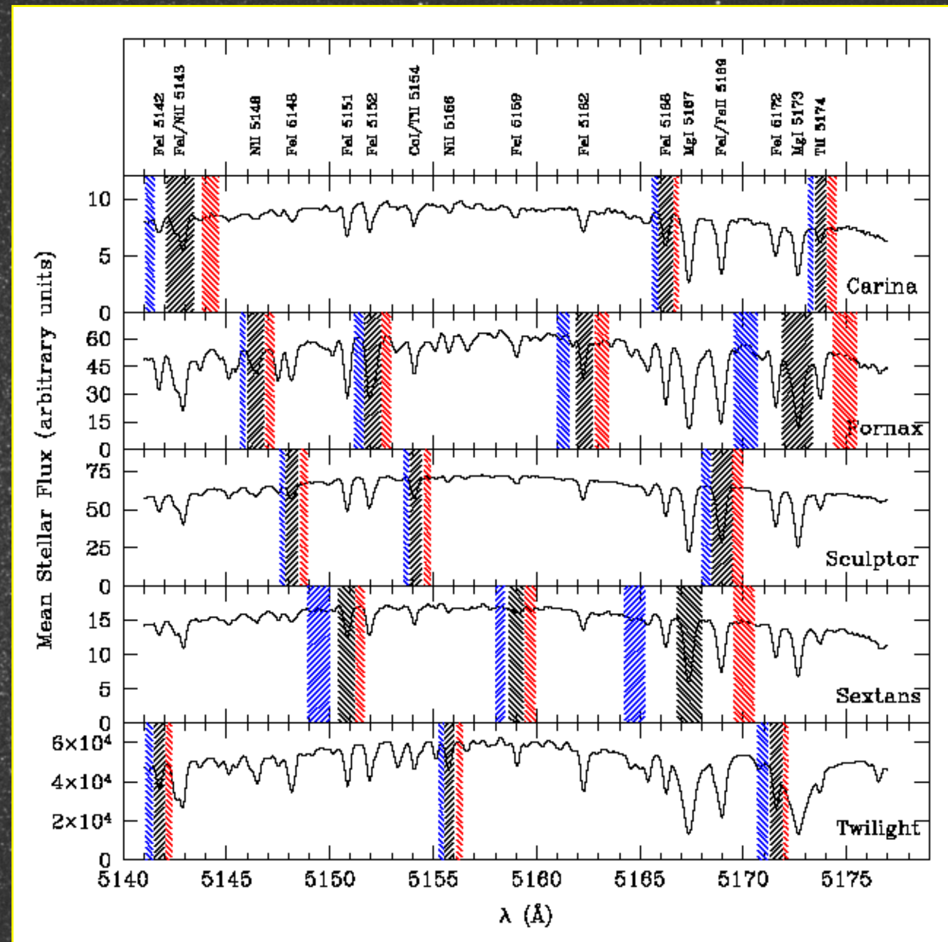

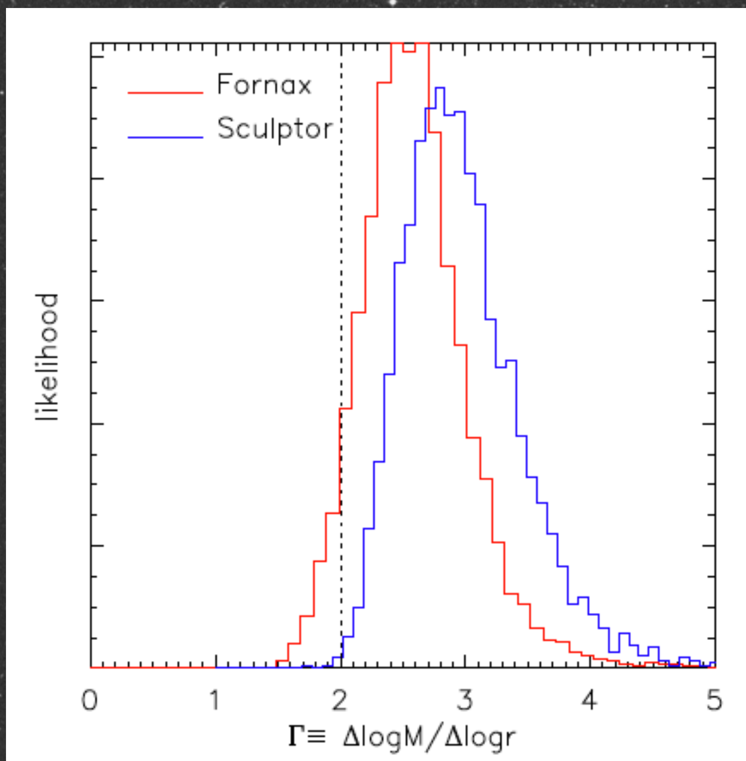

Fornax
Sculptor
likelihood
0
1
2
3
4
5
Γ≡ ΔlogM/Δlogr

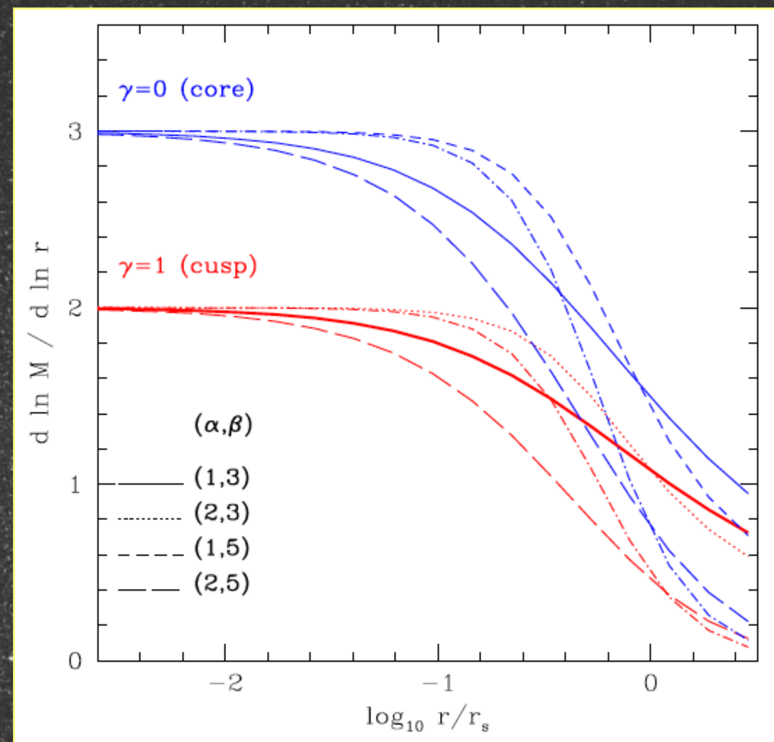

γ=0 (core)
γ=1 (cusp)
d ln M / d ln r
(α,β)
(1,3)
(2,3)
(1,5)
(2,5)
0
1
2
3
−2
−1
0
log10 r/rs

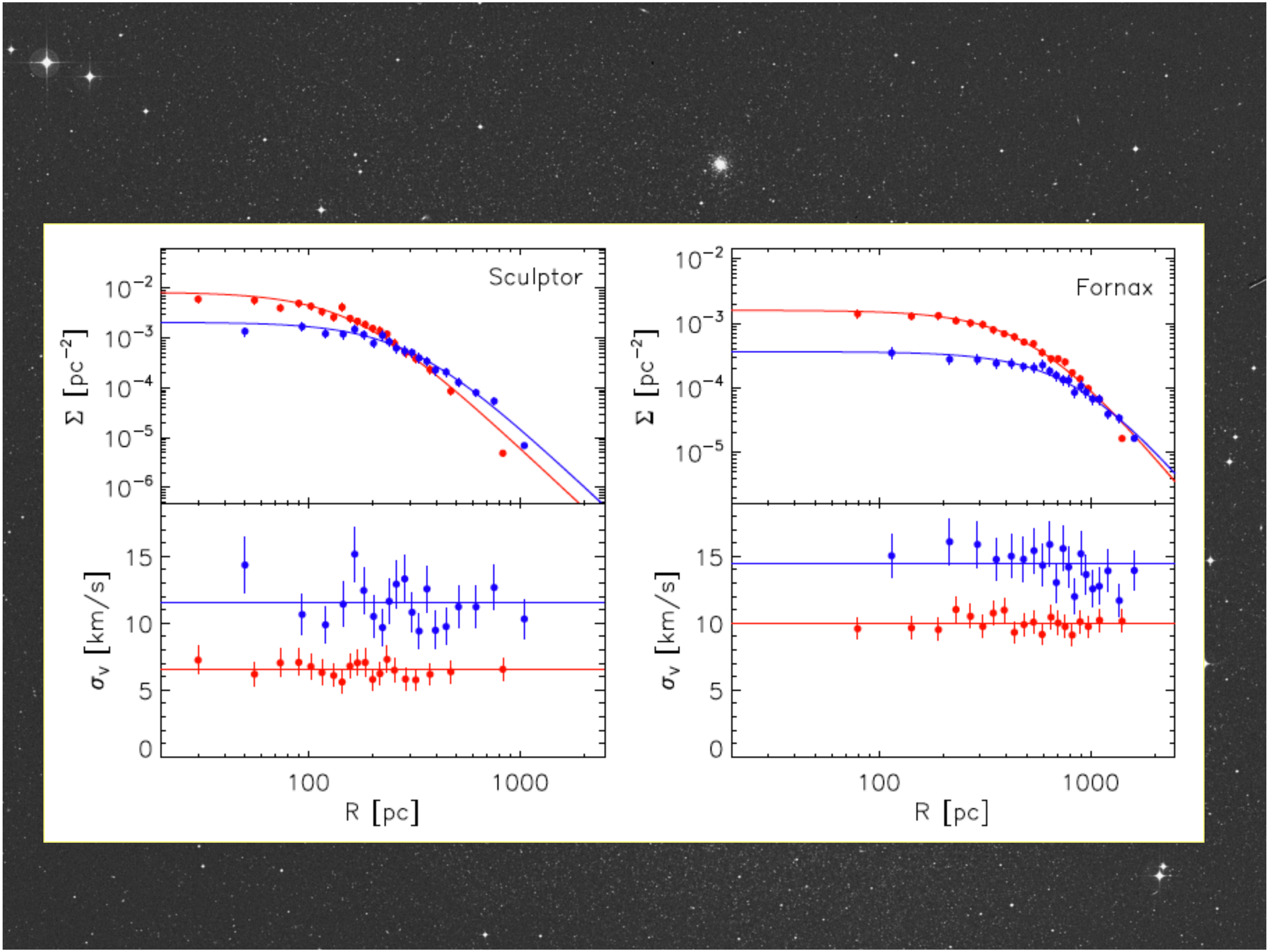
Sculptor
Fornax
Σ [pc⁻²]
σ_v [km/s]
R [pc]
100
1000
15
10
5
0

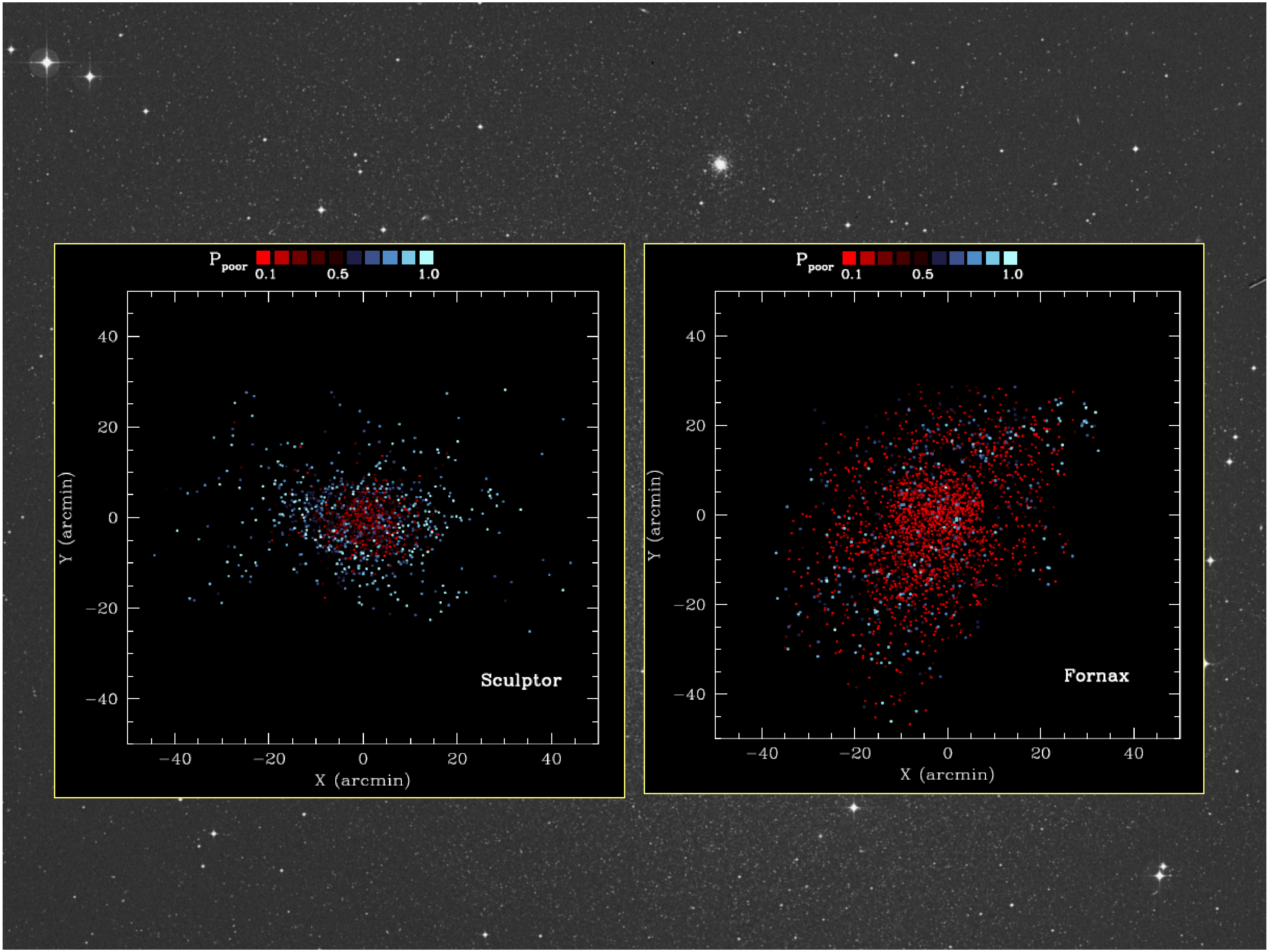

P poor
0.1
0.5
1.0
Y (arcmin)
X (arcmin)
Sculptor
Fornax

N-Body Simulations: Cusps

THE STRUCTURE OF COLD DARK MATTER HALOS

JOHN DUBINSKI AND R. G. CARLBERG
Department of Astronomy, University of Toronto, Toronto, Ontario, Canada M5S 1A1
Received 1990 December 26; accepted 1991 March 22

ABSTRACT

The density profiles and shapes of dark halos are studied using the results of *N*-body simulations of the gravitational collapse of density peaks. The simulations use from 3×10^4 to 3×10^5 particles, which allow density profiles and shapes to be well resolved. The core radius of a typical dark halo is found to be no greater than the softening radius, $\epsilon = 1.4$ kpc. The density profiles can be fitted with an analytical model with an effective power law which varies between -1 in the center to -4 at large radii. The dark halos have circular velocity curves which behave like the circular velocity contribution of the dark component of spiral galaxies inferred from rotation curve decompositions. The halos are strongly triaxial and very flat, with $\langle c/a \rangle = 0.50$ and $\langle b/a \rangle = 0.71$. There are roughly equal numbers of dark halos with oblate and prolate forms. The distribution of ellipticities in projection for dark halos reaches a maximum at $\epsilon = 0.5$, in contrast to the ellipticity distribution of elliptical galaxies, which peaks at $\epsilon = 0.2$.

Subject headings: dark matter — galaxies: structure — numerical methods

Dubinski & Carlberg (1991):
gamma ~1

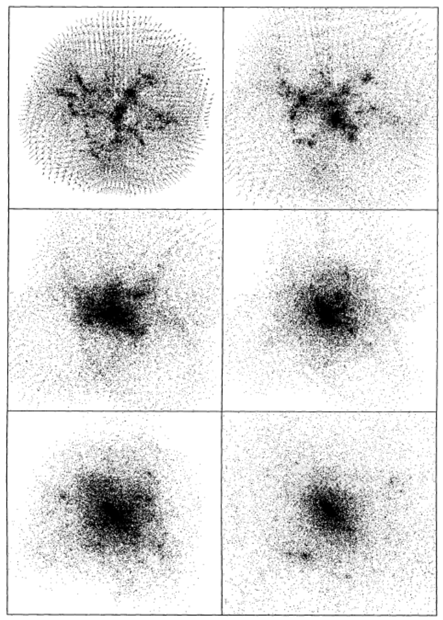

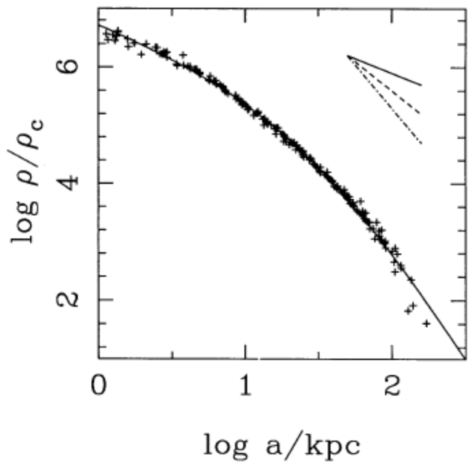

FIG. 2.—Density profiles of dark halos. Density is in units of the critical density ρ_c, and the elliptical radius a is in kpc. Thirteen points were used for the two-parameter fit of Hernquist's profile for each of the 14 halos. Each set of points has been renormalized to the fiducial Hernquist profile, with $r_s = 28$ kpc and $M_s = 2.1 \times 10^{12}\ M_\odot$ represented by the solid line. The lines in the upper right-hand corner present power-law slopes of -1, -2, and -3, respectively.

N-Body Simulations: Cusps

$$\frac{\rho(r)}{\rho_{\rm crit}} = \frac{\delta_c}{(r/r_s)(1 + r/r_s)^2}$$

NFW 1997: gamma =1

THE ASTROPHYSICAL JOURNAL, 490: 493–508, 1997 December 1

A UNIVERSAL DENSITY PROFILE FROM HIERARCHICAL CLUSTERING

JULIO F. NAVARRO[1]
Steward Observatory, 933 North Cherry Avenue, University of Arizona, Tucson, AZ 85721-0065; jnavarro@as.arizona.edu.

CARLOS S. FRENK
Department of Physics, University of Durham, South Road, Durham DH1 3LE, England; c.s.frenk@uk.ac.durham

AND

SIMON D. M. WHITE
Max-Planck-Institut für Astrophysik, Karl-Schwarzschild-Strasse 1, 85740, Garching bei München, Germany; swhite@mpa-garching.mpg.de

Received 1996 November 13; accepted 1997 July 15

ABSTRACT

We use high-resolution *N*-body simulations to study the equilibrium density profiles of dark matter halos in hierarchically clustering universes. We find that all such profiles have the same shape, independent of the halo mass, the initial density fluctuation spectrum, and the values of the cosmological parameters. Spherically averaged equilibrium profiles are well fitted over two decades in radius by a simple formula originally proposed to describe the structure of galaxy clusters in a cold dark matter universe. In any particular cosmology, the two scale parameters of the fit, the halo mass and its characteristic density, are strongly correlated. Low-mass halos are significantly denser than more massive systems, a correlation that reflects the higher collapse redshift of small halos. The characteristic density of an equilibrium halo is proportional to the density of the universe at the time it was assembled. A suitable definition of this assembly time allows the same proportionality constant to be used for all the cosmologies that we have tested. We compare our results with previous work on halo density profiles and show that there is good agreement. We also provide a step-by-step analytic procedure, based on the Press-Schechter formalism, that allows accurate equilibrium profiles to be calculated as a function of mass in any hierarchical model.

Subject headings: cosmology: theory — dark matter — galaxies: halos — methods: numerical

N-Body Simulations: Cusps

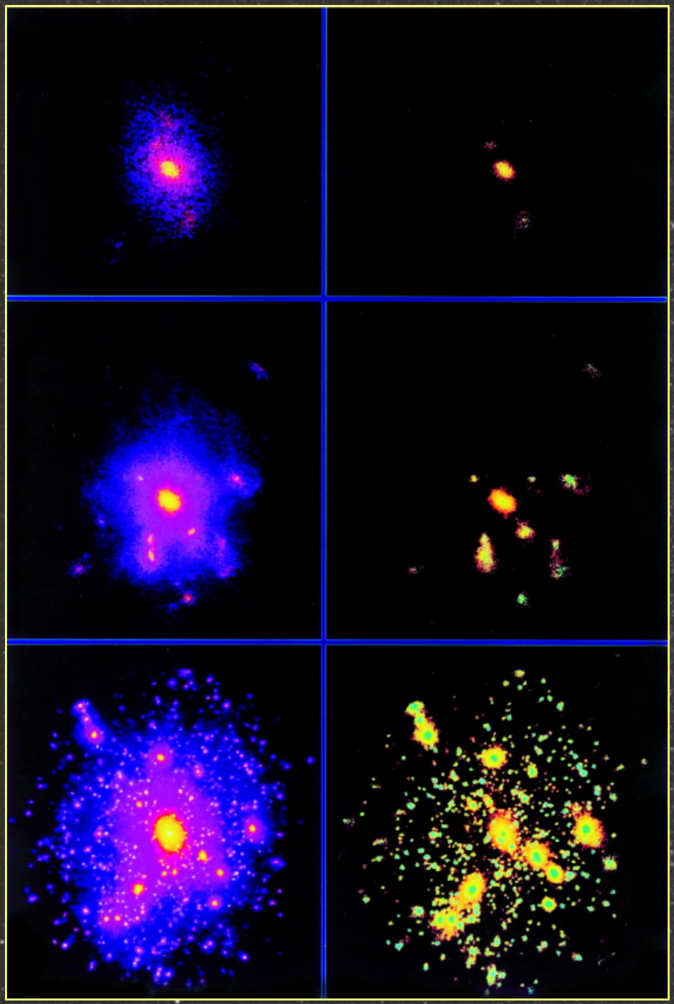

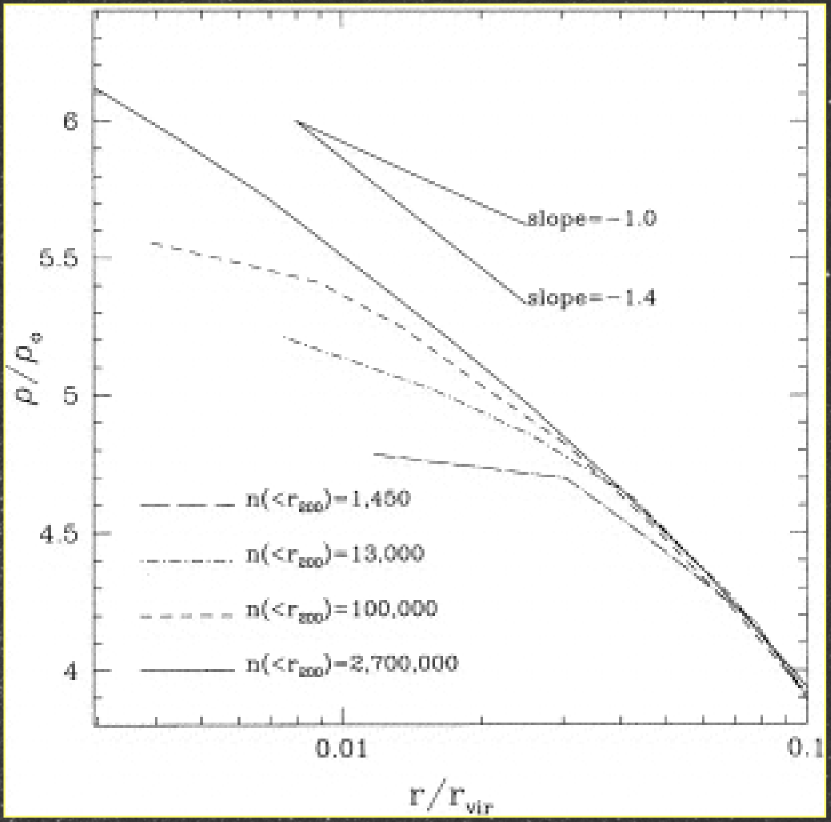

Moore etal. (1998) : gamma > 1, steeper cusp than NFW

N-Body Simulations: Cusps

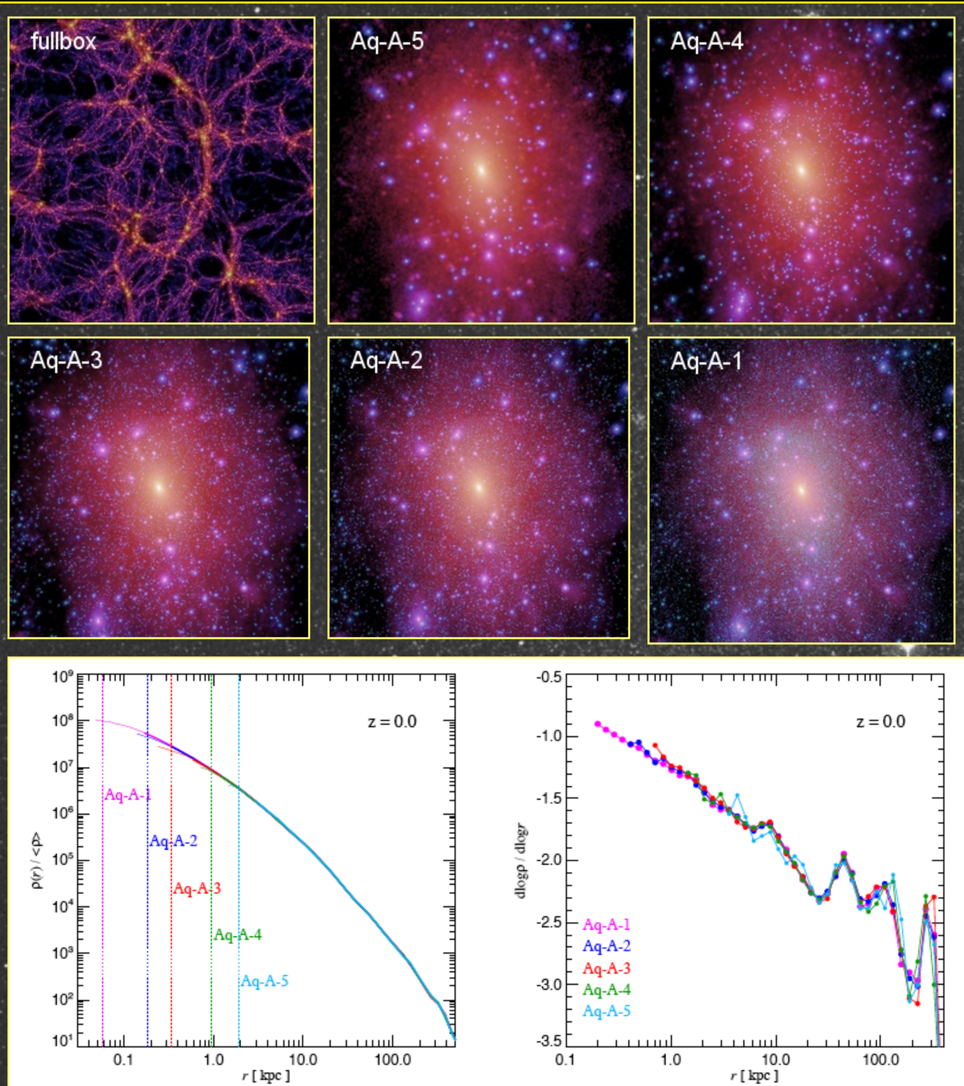

Springel etal. 2008: : gamma ~1
to at least R ~ 100 pc

Observations: Cores?

- Vcirc^2=GM/r
- Flat rotation curves --> dark matter
- Linear rise, flat in outer parts
- Well-fit by pseudo-isothermal sphere:

$$\rho_{\mathrm{PI}}(r) = \frac{\rho_0}{1+(r/R_C)^2}$$

- Notice: gamma = 0, beta=2 (not NFW)

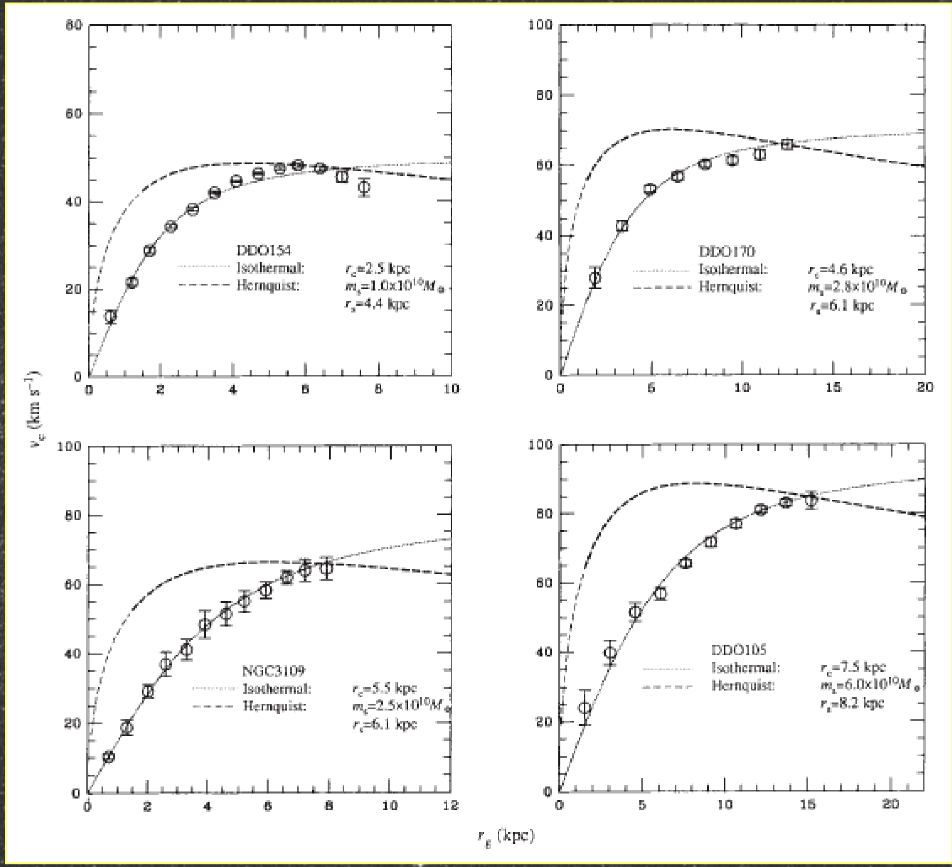

Moore (1994)

Observations: Cores?

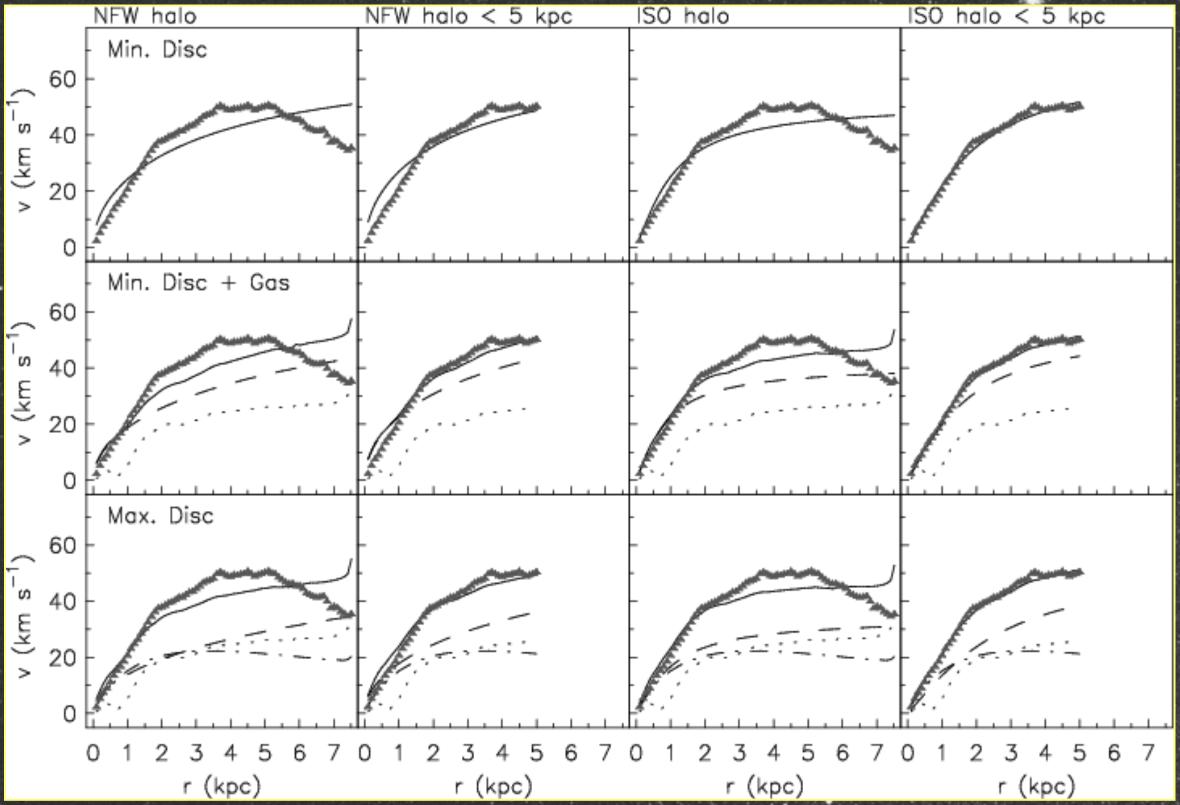

Van Eymeren etal. (2009)

- -Rotation curve analysis complicated by mass deconvolution
- -Stellar M/L typically dominates uncertainty
- -Now we see the value of low-surface-brightness galaxies!

Observations: Cores?

High-resolution rotation curves of low surface brightness galaxies*

W. J. G. de Blok[1] and A. Bosma[2]

[1] ATNF, CSIRO, PO Box 76, Epping NSW 1710, Australia
[2] Observatoire de Marseille, 2 place Le Verrier, 13248 Marseille Cedex 4, France

Received 18 July 2001 / Accepted 15 January 2002

Abstract. We present high-resolution rotation curves of a sample of 26 low surface brightness galaxies. From these curves we derive mass distributions using a variety of assumptions for the stellar mass-to-light ratio. We show that the predictions of current Cold Dark Matter models for the density profiles of dark matter halos are inconsistent with the observed curves. The latter indicate a core-dominated structure, rather than the theoretically preferred cuspy structure.

De Blok & Bosma (2002)

LSBs are DM-dominated, so Vcirc provides more direct measure of DM potential

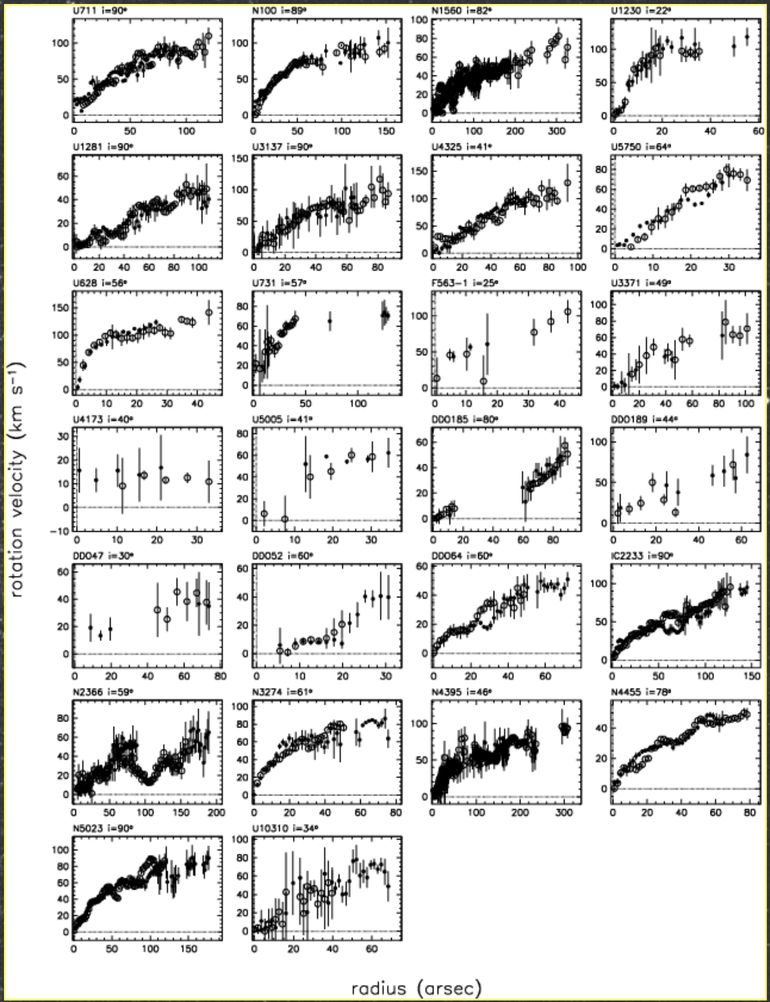

Creating Cores in Simulations

1996MNRAS.2

The cores of dwarf galaxy haloes

Julio F. Navarro,[1,2★] Vincent R. Eke[2] and Carlos S. Frenk[2]

[1]*Steward Observatory, The University of Arizona, Tucson, AZ 85721, USA*
[2]*Physics Department, University of Durham, South Road, Durham DH1 3LE*

Accepted 1996 September 2. Received 1996 August 28; in original form 1996 June 26

ABSTRACT
We use *N*-body simulations to examine the effects of mass outflows on the density profiles of cold dark matter (CDM) haloes surrounding dwarf galaxies. In particular, we investigate the consequences of supernova-driven winds that expel a large fraction of the baryonic component from a dwarf galaxy disc after a vigorous episode of star formation. We show that this sudden loss of mass leads to the formation of a core in the dark matter density profile, although the original halo is modelled by a coreless (Hernquist) profile. The core radius thus created is a sensitive function of the mass and radius of the baryonic disc being blown up. The loss of a disc with mass and size consistent with primordial nucleosynthesis constraints and angular momentum considerations imprints a core radius that is only a small fraction of the original scalelength of the halo. These small perturbations are, however, enough to reconcile the rotation curves of dwarf irregulars with the density profiles of haloes formed in the standard CDM scenario.

Navarro etal. (1996)

-Blowout of baryons can transform cusp into core as halo readjusts.

-BUT, this is more effective in dwarf galaxies than in deeper potential wells

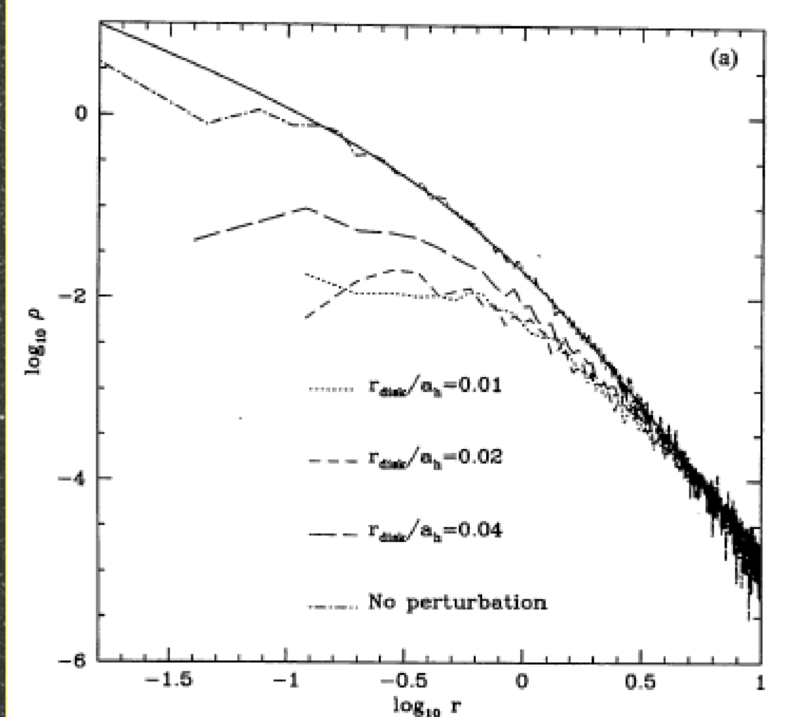

Creating Cores in Simulations

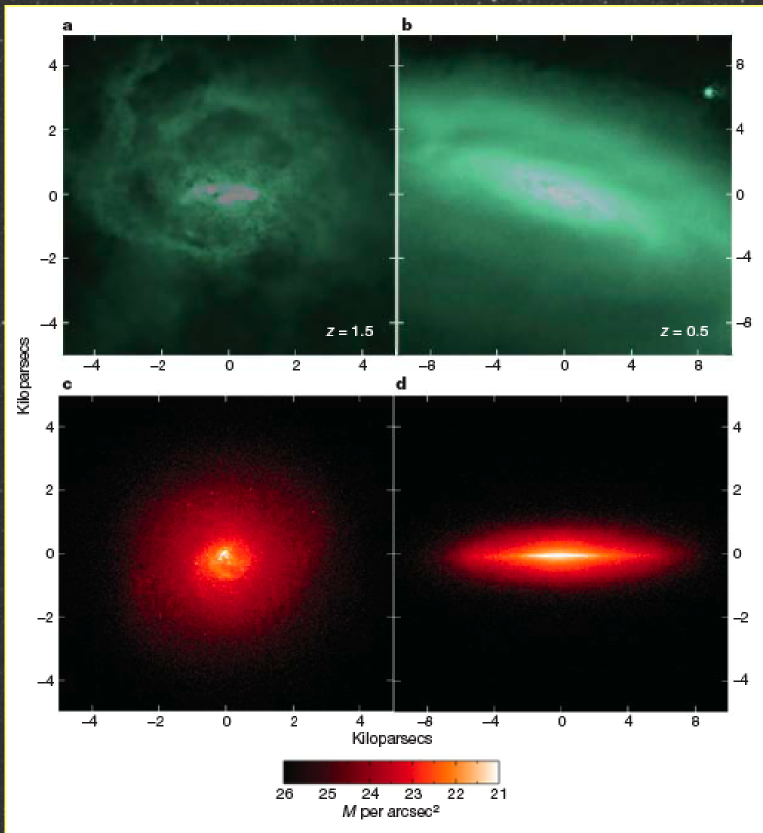

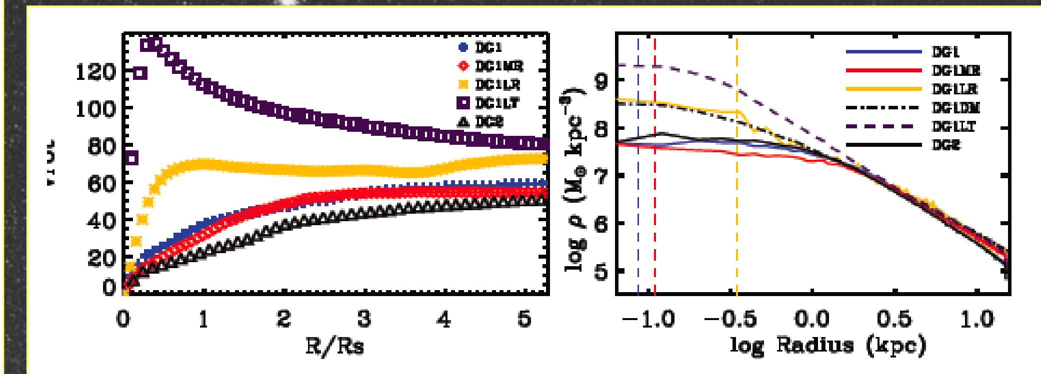

Governato etal. (2010)

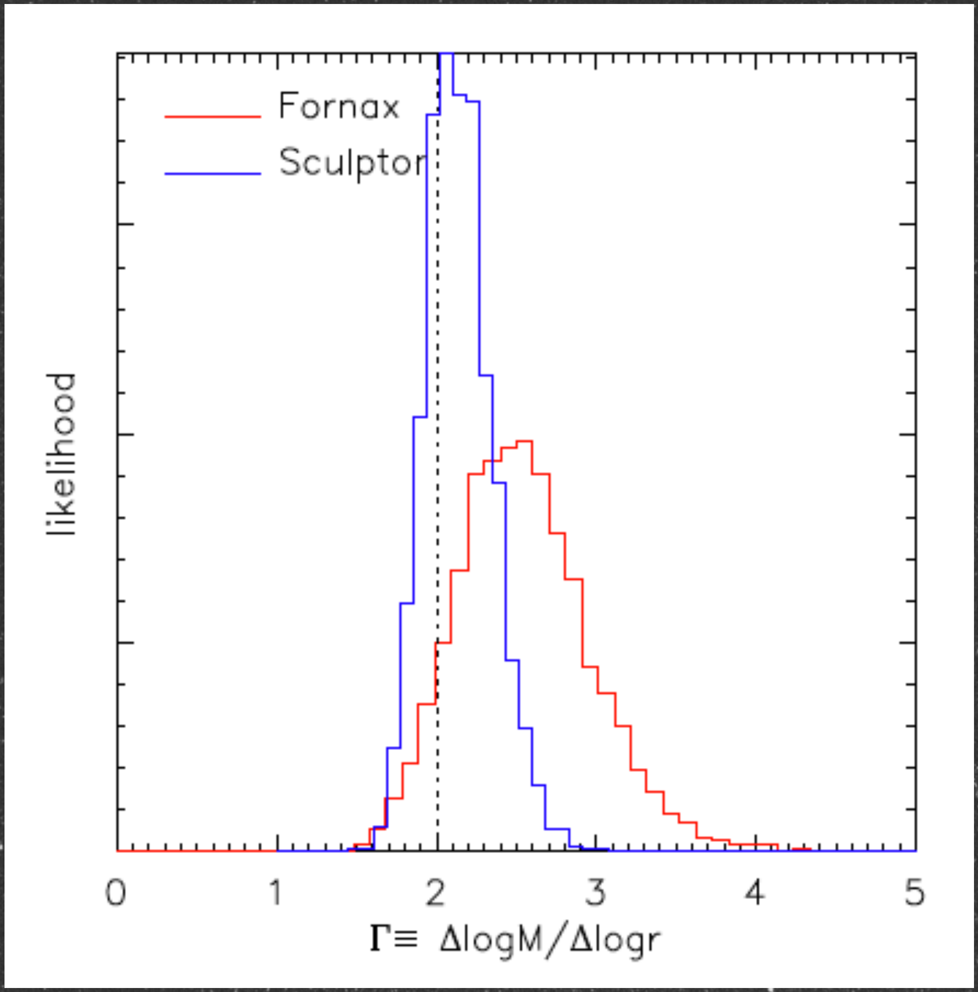

$$\Gamma \equiv \frac{\Delta \log M}{\Delta \log r} = \frac{\log[M(r_{\mathrm{h},2})/M(r_{\mathrm{h},1})]}{\log[r_{\mathrm{h},2}/r_{\mathrm{h},1}]} \approx 1 + \frac{\log[\sigma_{V,2}^2/\sigma_{V,1}^2]}{\log[r_{\mathrm{h},2}/r_{\mathrm{h},1}]}$$

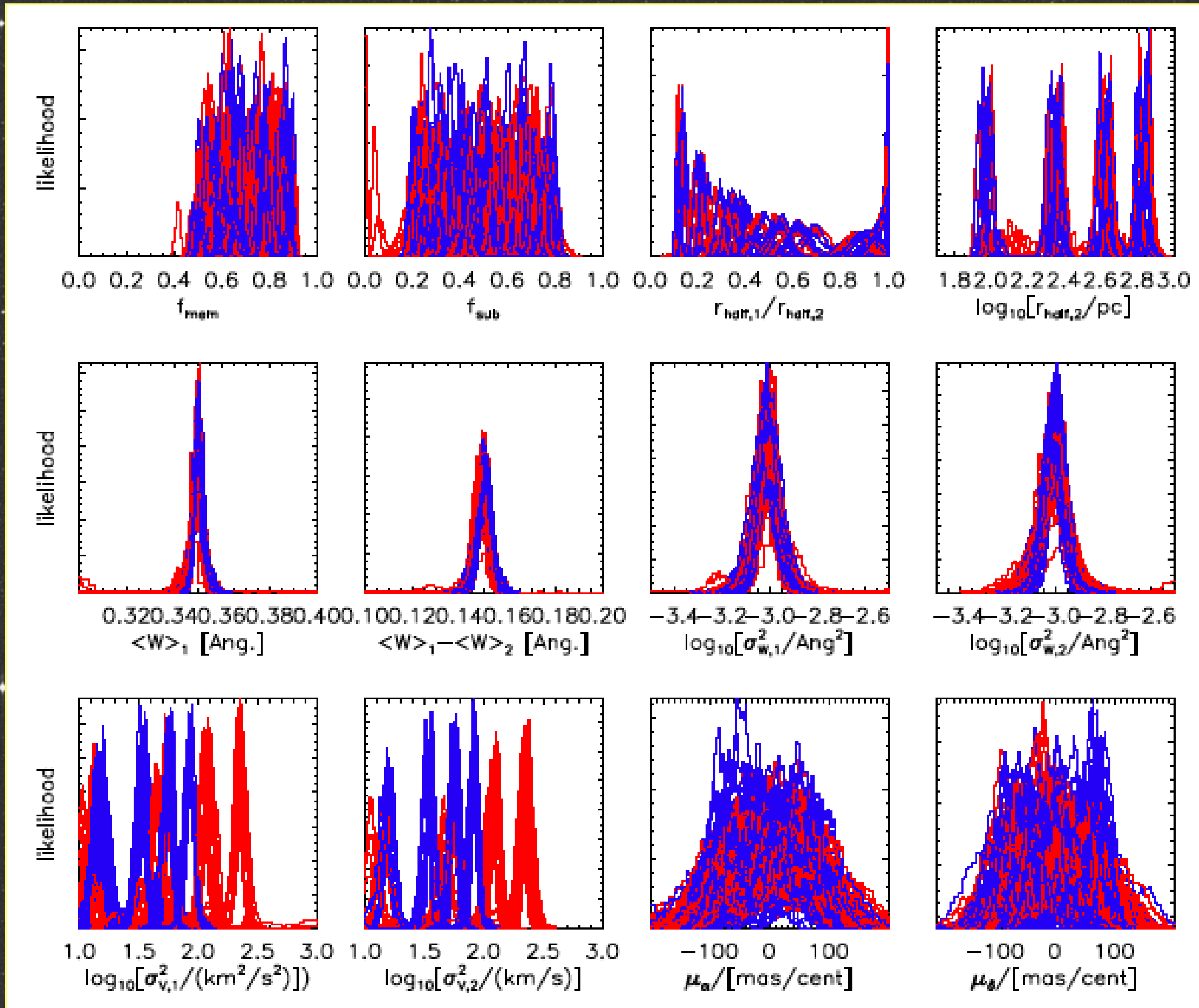

likelihood
0.0 0.2 0.4 0.6 0.8 1.0
f_{mem}
0.0 0.2 0.4 0.6 0.8 1.0
f_{sub}
0.0 0.2 0.4 0.6 0.8 1.0
$r_{half,1}/r_{half,2}$
1.8 2.0 2.2 2.4 2.6 2.8 3.0
$\log_{10}[r_{half,2}/pc]$
likelihood
0.32 0.34 0.36 0.38 0.40
<W>$_1$ [Ang.]
0.10 0.12 0.14 0.16 0.18 0.20
<W>$_1$−<W>$_2$ [Ang.]
−3.4 −3.2 −3.0 −2.8 −2.6
$\log_{10}[\sigma^2_{W,1}/Ang^2]$
−3.4 −3.2 −3.0 −2.8 −2.6
$\log_{10}[\sigma^2_{W,2}/Ang^2]$
likelihood
1.0 1.5 2.0 2.5 3.0
$\log_{10}[\sigma^2_{V,1}/(km^2/s^2)]$)
1.0 1.5 2.0 2.5 3.0
$\log_{10}[\sigma^2_{V,2}/(km/s)]$
−100 0 100
μ_α/[mas/cent]
−100 0 100
μ_δ/[mas/cent]

What About Dwarf Spheroidals?

- All of the above concerned relatively massive galaxies, even the LSBs and the cored dwarf galaxies created by Governato etal.
- dSphs are less massive by several orders of magnitude
- dSphs have much smaller baryon content --> more ‘pristine’ DM halos?
- dSphs are supported by velocity dispersion, not rotation --> cannot measure Vcirc directly

Observations: Cores?

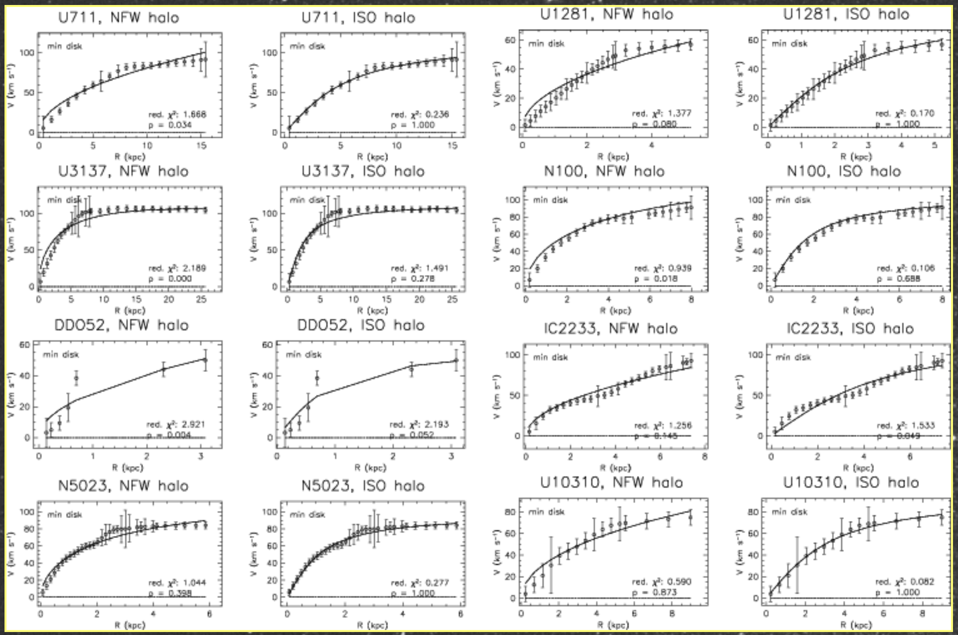

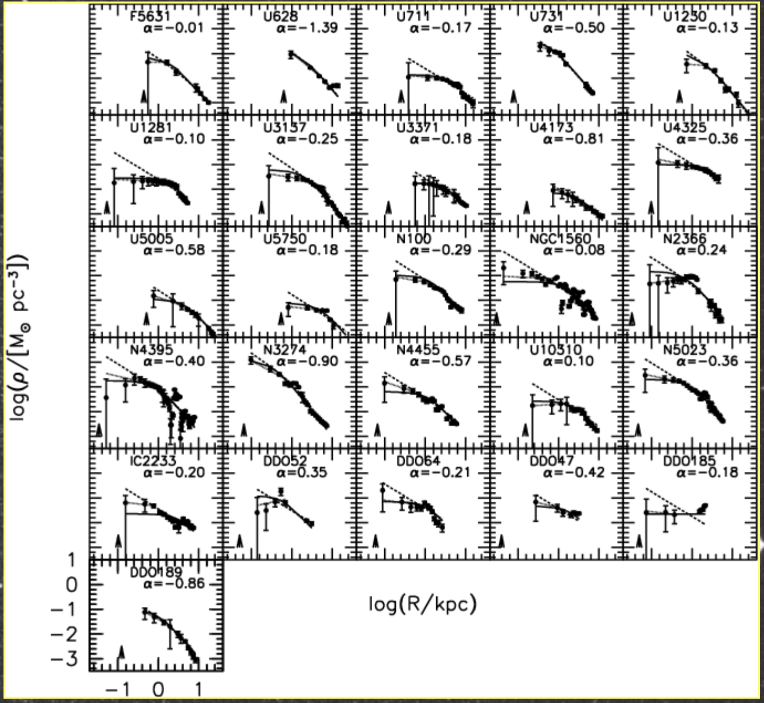

de Blok & Bosma (2002)

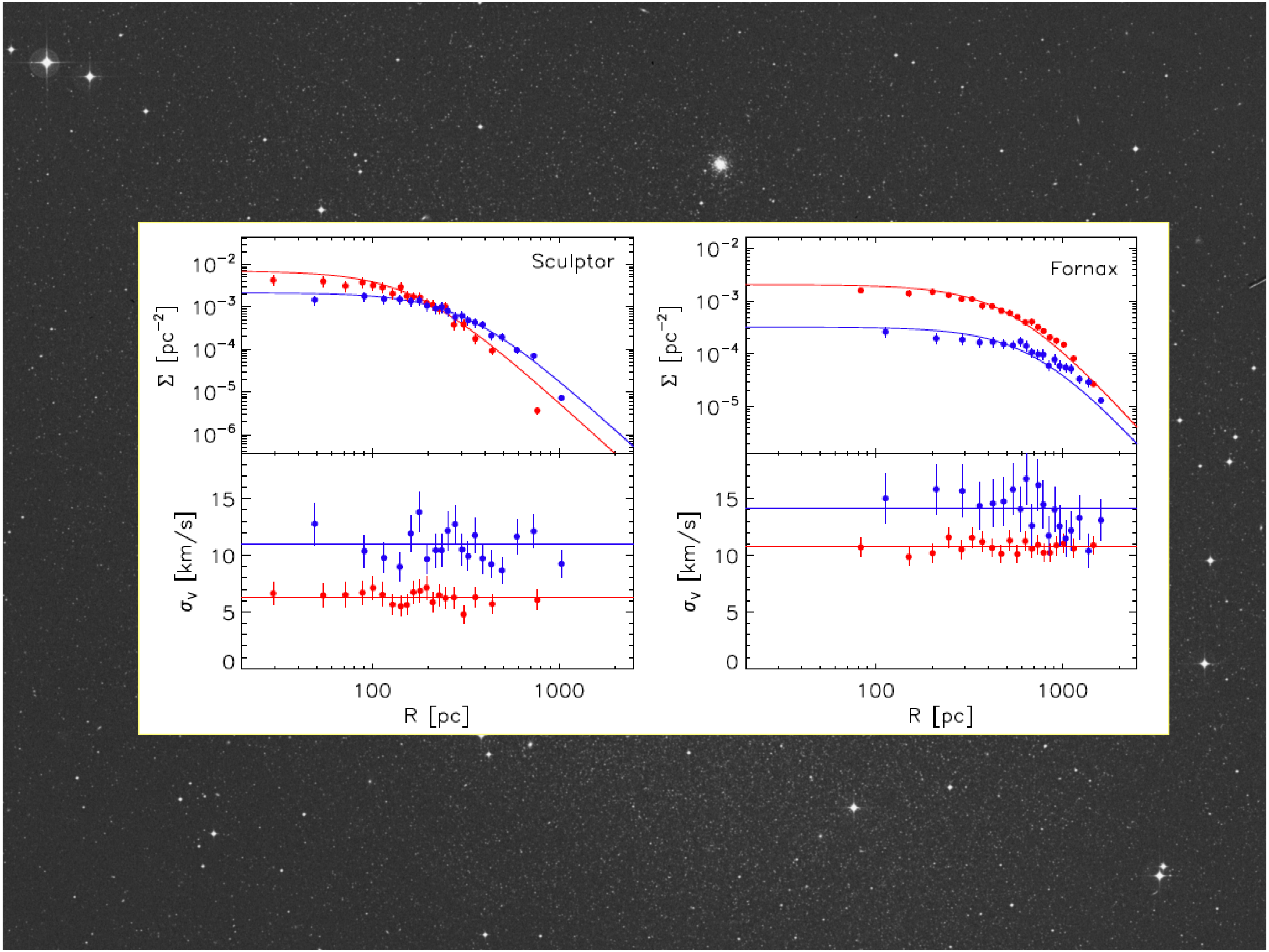

Sculptor
Fornax
Σ [pc^−2]
σ_v [km/s]
R [pc]
10^−2
10^−3
10^−4
10^−5
10^−6
15
10
5
0
100
1000